Microchim Acta (2015) 182:1567–1589
DOI 10.1007/s00604-015-1504-x

REVIEW ARTICLE

Multifunctional hydroxyapatite nanoparticles for drug delivery and multimodal molecular imaging

Sasidharanpillai S. Syamchand[1] · **George Sony**[1]

Received: 29 January 2015 / Accepted: 17 April 2015 / Published online: 23 May 2015

Abstract Hydroxyapatite (HAp) is the most important constituent of biological tissues such as bone and teeth and exhibits several characteristic features. HAp nanoparticles (NPs) are good host materials and can be functionalized with various kinds of dopants and substrates. By endowing HAp NPs with desired properties in order to render them suitable for biomedical applications including cellular imaging, non-invasive and quantitative visualisation of molecular process occurring at cellular and subcellular levels becomes possible. Depending on their functional properties, HAp based nanoprobes can be divided into three classes, i.e., luminescent HAp NPs (for both downconversion and upconversion luminescence), magnetic HAp NPs, and luminomagnetic HAp NPs. Luminomagnetic HAp NPs are particularly attractive in terms of bimodal imaging and even multimodal imaging by virtue of their luminescence and magnetism. Functionalised HAp NPs are potential candidates for targeted drug delivery applications. This review (with 166 references) spotlights the cellular imaging applications of three types of HAp NPs. Specific sections cover aspects of molecular imaging and the various imaging modes, a comparison of the common types of nanoprobes for bioimaging, synthetic methods for making the various kinds of HAp NPs, followed by overviews on fluorescent NPs for bioimaging (such as quantum dots, gold nanoclusters, lanthanide-doped or fluorophore-doped NPs), magnetic HAp NPs for use in magnetic resonance imaging (MRI), luminomagnetic HAp NPs for bimodal imaging, and sections on drug delivery as well as cellular imaging applications of HAp based nanoprobes (including targeted imaging).

Keywords Hydroxyapatite nanoparticles · Nanoprobes · Drug delivery · Molecular imaging · Multimodal imaging · Targeted imaging

Introduction

Hydroxyapatite [HAp; $Ca_{10}(PO_4)_6(OH)_2$] is the main constituent of biological tissues such as vertebrate bone and teeth. HAp exhibits several characteristic features of an ideal natural biomaterial such as excellent biocompatibility, biodegradability, bioresorability, osteogenisis, osteoconductivity and osteoinductivity [1–3]. Synthetic HAp has been preferred as the material for hard tissue repair. It is effective in reducing aseptic loosening associated with post-implant surgery [4]. Nanophase HAp possesses unique properties such as high surface to volume ratio, reactivity and biomimetic morphologies compared to bulk counterpart due to quantum size effect and surface phenomena at the nanolevel [5]. HAp nanocrystals found enormous applications in the field of tissue engineering, nanomedicine, industrial catalysis and in many other disciplines [6, 7]. HAp nanoparticles are more favourable in applications like orthopaedic implant coating. It has been observed that HAp NPs can significantly enhance the biocompatibility and bioactivity of synthetic biomaterials.

HAp nanospheres can act as carriers for controlled drug delivery [8]. Encapsulation of drugs within HAp matrix or coupled to HAp NPs enable targeted drug delivery. Nanoparticulate carriers based on HAp are desirable for both systemic and localised drug delivery particularly due to their solubility in vivo and capacity to penetrate the cell membranes [9]. However the difficulty associated with the loading of

✉ George Sony
emailtosony@gmail.com

[1] Department of Chemistry, University of Kerala, Kariavattom Campus, Trivandrum 695 581, Kerala, India

drugs that are insoluble in water may limit the application of HAp as a nanocarrier [10]. HAp NPs exhibit considerable anticancer activity, since studies revealed that HAp can inhibit the growth of many kinds of cancer cells [6, 11, 12]. Several reports on antimicrobial effects of HAp based nanoprobes are available. Silver ions can offer antibacterial activity to HAp NPs, due to the interaction of silver ions with the thiol functional group in bacterial proteins [13, 14]. The biocompatibility of HAp NPs is widely accepted by the scientific community with a little controversy. Very recently in vitro studies on the interaction of HAp NPs with bone marrow mesenchymal stem cells (BMSCs) revealed excellent biocompatibility of HAp NPs [15]. Few reports about the cytotoxicity of HAp nanocrystals are available and it has been observed that cytotoxicity of HAp NPs is shape and cell dependent [16]. Even though HAp NPs are associated with several favourable features for biomedical and other applications, the precise control of size and shape to produce uniform NPs is a challenge and it limit their applications.

HAp nanocrystals are good host for many materials and can be doped with dyes, different metal ions including lanthanide ions and other substrates. HAp NPs doped with suitable materials may exhibit different functional properties, which make them adaptable for bioimaging and other applications. Bioimaging is widely used in biomedical sciences for applications ranging from the morphological analysis of anatomical structures to sensitive measurements of intracellular molecular events [17, 18]. The function of HAp based nanoprobes in bioimaging is highly promising and the present review focuses on the bioimaging applications of HAp based nanoprobes.

Molecular imaging and different imaging modes

In this section we shall consider various imaging modes including multimodal imaging and nanoprobes commonly employed in bioimaging. The two major applications of nanomaterials in the biomedical field are imaging and therapy. This is mainly because of the fact that nanomaterials can overcome the shortcomings such as short-blood circulation time and non-specific bio distribution associated with conventional imaging and therapeutic probes. For instance the blood circulation time can be increased by the control of size of nanomaterials and specific bio distribution can be accomplished by conjugating nanomaterials with specific targeting moieties [19, 20]. Molecular imaging is a rapidly emerging tool in the clinical discipline and myriad advances have been made to make this technique as a most powerful diagnostic procedure. The molecular imaging aimed at non-invasive and quantitative visualisation of molecular process occurring at cellular and sub cellular levels.

The common imaging modes include magnetic resonance imaging (MRI), X-ray computed tomography (CT), positron emission tomography (PET), single photon emission computed tomography (SPECT), optical coherence tomography (OCT), optical imaging (OI) including NIR and upconversion (UC) luminescence imaging, ultrasound and photoacoustic imaging [21]. It has been observed that various imaging modes differ in key characteristic features such as spatial resolution, soft tissue contrast, tissue penetration limit, imaging time and sensitivity. Various common imaging modes and their characteristic features are given in Table 1.

It has been observed that the imaging modes CT, PET and SPECT are radiodiagnostic techniques and are prone to radiation risks. Compared to the radiodiagnostic techniques PET and SPECT, MRI has significantly high spatial resolution but MRI contrast agents (CA) should be used in large concentrations ($\sim 10^{-5}$ M) to achieve desired contrast enhancement [22].

Multimodal imaging (MMI)

MMI has emerged as a technology that utilises the strengths of different modes and yields a hybrid imaging platform with benefits superior to any of its individual components [34]. It can offer complementary advantages like high spatial resolution and soft tissue contrast. Combination of different nanostructured materials with different functional properties can offer synergistic multifunctional properties, which enable MMI. However incorporation of different modes in a single probe may create difficulties such as targeting, different concentration requirements for different contrast agents, stability and concern about biocompatibility. Recently, researchers focused on MMI combined with therapeutics to obtain theranostic nano systems with wide applicability. It has been observed that in most of the multimodal imaging systems MR, PET or optical imaging is one component and CT based systems are limited due to high concentration requirement of contrast agents for CT. The area of MRI/optical imaging is well developed in terms of dual-modality imaging [35, 36]. Several reports came on bimodal imaging modes like PET/CT and PET/ MRI. Among these bimodal systems, PET/MRI is more preferred due to the fact that MRI can provide more robust imaging evaluation in clinical settings. Moreover PET/CT systems fail to perform simultaneous data acquisition and also limited by significant radiation dose contributed by CT [37, 38]. Upconversion luminescence systems are recently employed in multimodal imaging by combination with other modes [39].

Nanoprobes for bioimaging

A wide variety of nanoparticles are used as bioimaging probes and a large volume current research is emerging towards the

Table 1 Selected imaging modes and their characteristic features

Imaging modality	Key features	Spatial Resolution	Ref.
Magnetic resonance imaging (MRI)	High spatial resolution; low sensitivity; having no tissue penetration limit and long imaging time. Relatively large local concentration of the contrast agent (CA) is required to achieve the contrast enhancement; detects the magnetic field	25–100 μm	[21, 22]
X-ray computed tomography (CT)	High spatial resolution; low resolution for soft tissues; short imaging time and no tissue penetration limit; detect X-rays	50–200 μm	[23, 24]
Positron emission tomography (PET)	Highly sensitive imaging modality; can detect only radionuclide; no tissue penetration limit; detect gamma rays	~ 2 mm	[25, 26]
Single photon emission computed tomography (SPECT)	Highly sensitive; no tissue penetration limit; low spatial resolution; detect gamma rays	~ 2 mm	[27]
Optical coherence tomography (OCT)	Provide cross sectional sub-surface imaging of biological tissue; high spatial resolution; detects photons in NIR region	50 μm	[28, 29]
Optical imaging (OI)	Low spatial resolution; poor penetration depth; multicolour imaging is highly sensitive; detects the photons in the visible or NIR region	2–5 mm	[21, 30]
Ultrasound imaging	Poor image contrast; not suitable for air containing organs; detects ultrasonic waves	50–500 μm	[31, 32]
Photoacoustic imaging	High spatial resolution; better depth resolution than light; based on photoacoustic effect	50 μm	[33]

prospecting of novel nanoprobes with improved performance in bioimaging including multimodal imaging. Several nanoparticles as such employed in bioimaging by virtue of their certain characteristic features like luminescence, magnetism etc. For instance gold nanostructures (nanoparticle, nanorod, nanoshell, nanocage, nanoclusters) are highly useful in optical imaging due to their inherent luminescent properties; oxide nanoparticles (Fe_2O_3, Gd_2O_3 etc.) used as contrast agents in MRI due to inherent magnetism. However the incorporation of several components into nanoparticle matrix enables the formation of efficient nanoprobes for bioimaging. For instance dye doped silica NPs can be used in optical imaging due to the luminescence of the dye component; dendrimers can be used as nanoprobes for bioimaging such as fluorescence imaging, CT, PET and MRI by the incorporation of reporter moieties [40]. Figure 1 illustrates the important reporter moieties of nanoparticles as well as pristine nanoparticles used as imaging probes in different modes.

Among various imaging modes, MRI and OI are very common methods that utilise a wide variety of nanoparticles as imaging probes. Several reviews on nanoprobes for MRI are available in literature. The nanoparticles commonly used for optical imaging has been reviewed recently [41]. Table 2 gives representative examples of particles other than HAp NPs for use in OI and MRI.

Even though a large number of nanoprobes are developed for the bioimaging applications, their practical utility is limited by several factors. Such factors mainly include the stability, hydrophilicity/ hydrophobicity, precise size control, biocompatibility, attachment of the targeting molecules and difficulties associated with the fabrication of the nanoprobes. For HAp based nanoprobes, most of the mentioned factors are favourable in view point of bioimaging. Pristine HAp NPs lack inherent functional features like luminescence or magnetism, essential for developing nanoprobes for bioimaging. However, incorporation of reporter moieties into the HAp nanomatrix either as dopant or as attachment can make HAp NPs adaptable for cellular imaging.

Synthesis and characterization of HAp based nanoprobes

In this section we shall mainly consider the synthetic strategies adopted for the fabrication of nanocrystalline HAp with different functional properties like luminescence and magnetism, for biomedical applications such as drug delivery and bioimaging. HAp is the thermodynamically more stable form of calcium phosphate in the physical environment (pH ≥ 5.4) [51]. The features of HAp nanocrystals like bioresorability, strength, toxicity etc. depend on the morphology, stoichiometry (Ca/P ratio) and phase purity. Various methods employed for the preparation of nanometric HAp as well as the

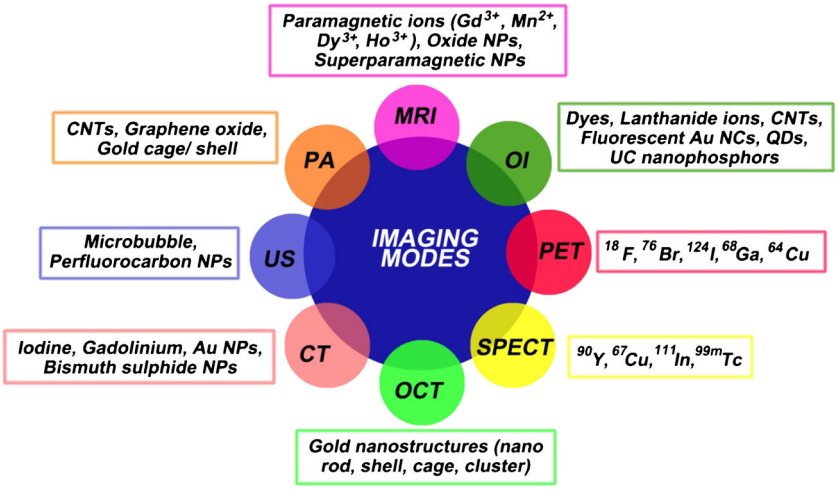

Fig. 1 Imaging probes/reporter moieties used in different imaging modes

advantages and disadvantage of such methods have been reviewed [52]. The size, morphology, degree of crystallinity, phase purity and Ca/P ratio depends on the method adopted for the synthesis as well as synthesis conditions. One of the noticeable features of the nanocrystalline HAp is their diverse morphology. Figure 2 represents common morphologies of nanocrystalline HAp. The common morphologies of HAp nanocrystals include nanorods, nanospheres, nanospindles, nanoflakes, nanoflowers and porous/mesoporous nanospheres. In majority of cases HAp NPs exhibit rod -like morphology and this structure is common for HAp NPs for biological applications.

The Ca/P ratio is an important parameter, which has strong implication on the biological applications of HAp NPs. Natural HAp exhibits a Ca/P ratio of 1.67 and calcium phosphate can be present in other important chemical phases also. Some important phases are octacalcium phosphate (Ca/P=1.3), dicalcium phosphate (Ca/P=1), β-tricalcium phosphate (Ca/P=1.5) and amorphous calcium phosphate (Ca/P=1.2–2.2) [5]. The Ca/P ratio of HAp NPs may vary with method of synthesis.

The common methods of synthesis of HAp NPs are (a) wet chemical synthesis (b) dry synthesis and (c) high temperature synthesis.

Wet chemical synthesis

Wet chemical methods are the most promising method for the fabrication of nanocrystalline HAp, since we can control the morphology as well as the size of the NPs. Low crystallinity of the NPs is a main disadvantage of this method. Most of the NPs included in the biological applications are synthesized by this method. The wet chemical method involves chemical precipitation (co-precipitation), hydrolysis, sol–gel synthesis, emulsion method and sonochemical synthesis [53]. It has been observed that in the wet chemical synthesis a lower processing temperature and higher stirring rate yields smaller HAp NPs [54].

Dry synthesis

Dry method involves solid-state method and mechanochemical synthesis. The dry methods produce NPs with diverse structure and high crystallinity. These methods do not require precisely controlled conditions, because such methods are almost independent of processing conditions.

High temperature synthesis

The high temperature synthesis can be by combustion and pyrolysis. High temperature syntheses also produce NPs with diverse structure in nanometric dimensions.

In addition to the mentioned methods, HAp nanocrystals can also be prepared by combination methods and from biogenic sources. In the combination method, two or more general methods are combined to get more efficiency in the synthesis. For instance sol–gel and combustion methods can be combined t get a synergistic effect in synthesis [55, 56]. HAp NPs can be obtained from various biogenic resources like bone waste, egg shell etc. But the resultants HAp NPs have large particle size [57]. The elemental composition and crystallinity of the synthesized HAp NPs can be characterised by routine methods, energy dispersive X-ray (EDX) analysis and X-ray powder diffraction (XRD) studies. The morphologies of HAp NPs synthesized by various methods can be analysed by using common nanometric characterisation methods like atomic force microscopy (AFM), scanning electron microscopy (SEM) and transmission electron microscopy (TEM).

The mesoporous HAp NPs with controlled pore size are highly useful in drug delivery applications. The porous structure enables the efficient drug loading in HAp NPs. The drug loaded mesoporous HAp NPs are efficient nanoprobes for controlled drug release triggered by different external factors

Table 2 Representative kinds of nanoparticles for use in optical imaging (OI) and magnetic resonance imaging (MRI), and their characteristic features

Nanosystems	Used in	Key features	Ref.
Fluorescent silica NPs	Optical imaging	NPs with controlled size can be prepared by simple methods; low cytotoxicity and good biocompatibility; can be doped with a number of fluorescent labels such as metallic, meta-organic and organic fluorophores; surface modification is possible; excellent cell imaging capability	[41, 42]
Hydrophilic polymers and hydrophobic organic polymers	Optical imaging	The emission wavelength of hydrophilic polymer NPs can be tuned between 300 and 1000 nm by changing dopants; tunable decay time and size; NPs undergo swelling in water but not tend to aggregate; certain hydrogels are highly promising nanosensors for fluorescent imaging of physiological pH. Hydrophobic organic polymers such as polystyrene NPs can be doped with lipophilic materials; size and decay time are tunable; good cell permeability and low cytotoxicity	[41, 43]
Polymer dots(P-dots), carbon dots (C-dots) and quantum dots (Q-dots)	Optical imaging	P-dots are prepared from aromatic precursors; the backbone of conjugated polymers act as light harvesting units; doping with fluorophores is not required; fluorescence ranges to NIR region; highly inert and do not swell in water. C-dots are the clusters of carbon atoms with diameter less than 8 nm; can be made fluorescent and need not be doped; emission colour can be tuned Q-dots are discussed in the section 'Fluorescent labels for fabrication of NPs for bioimaging'	[41, 44, 45]
Upconversion nanoparticles (UCNPs)	Optical imaging	UCNPs generally obtained from $NaYF_4$ nanocrystals duly doped with lanthanide ions; doping with flurophore not required; display several emission colours; size is tunable	[46]
Noble metal (Ag and Au) NPs and nanoclusters	Optical imaging	Ag and Au NPs display week fluorescence; the clusters are luminescent and good candidates for fluorescent imaging; they preferred in bioimaging due to inertness; modified nanoclusters enable targeted imaging	[41, 47]
Gadolinium chelates	Magnetic resonance imaging	Most widely used contrast agents based on T1 relaxation; number of chelates are available and largely used one is Gd-DTPA chelate(DTPA- diethyltriamine pentaacetic acid); Gd itself is toxic in ionic form; when administrated in a complex form its stability is influenced by temperature, pH, concentration of surrounding ions and ligands.	[48, 49]
Iron oxide NPs	Magnetic resonance imaging	They are designated according to their size and they may be superparamagnetic iron oxide NPs(SPIO) with particle size > 50 nm and ultra small superparamagnetic iron oxide NPs(USPIO) with particle size < 50 nm; they act as contrast agents based on T2 relaxation	[50]
Dysprosium and holmium complexes	Magnetic resonance imaging	Dy^{3+} and Ho^{3+} have very short electronic relaxation time due to their highly anisotropic ground state; Dy^{3+} and Ho^{3+} complexes are efficient T2 contrast agents in intermediate and high magnetic field strengths.	[22]

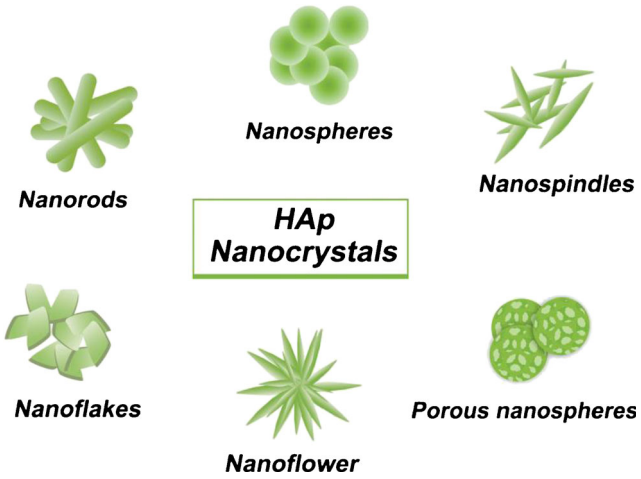

Fig. 2 Common morphologies of HAp nanocrystals

like pH. It has been observed that hydrothermal method and combustion method are generally employed for the preparation of porous HAp NPs [52].

Whatever may be the synthetic method adopted the precise control of size and morphology of the HAp NPs is difficult. Moreover, every synthetic procedure has advantages and disadvantages in connection with particle agglomeration, size distribution, phase impurities that may occur in crystal structure, diverse materials needed and economy in procedure. Therefore these factors should be considered while adopting a typical procedure for the synthesis of HAp NPs.

HAp based nanoprobes for drug delivery and cellular imaging

It has been observed that HAp NPs with different functional properties are employed as potential candidates for drug delivery applications. The drug delivery applications of HAp based nanoprobes are discussed in a separate section. HAp based nanoprobes can be conveniently divided into three types: luminescent HAp, magnetic HAp and luminomagnetic HAp nanoparticles (NPs) depending on the properties that are being explored in bioimaging. These three kinds of NPs shall be discussed in the following.

Luminescent HAp nanoparticles

The incorporation of at least one fluorescent label in the HAp matrix enables the formation of luminescent HAp NPs. For expediency, it is more appropriate to run through the advantages and shortcomings of various fluorescent labels as well as the mechanism of luminescence in luminescent NPs prior to the detailed discussion on luminescent HAp NPs.

Fluorescent labels for fabrication of NPs for bioimaging

The common fluorescent labels used in the fabrication of luminescent NPs for bioimaging include (a) organic dyes (b) quantum dots (c) gold nanoclusters and (d) lanthanide ion dopants. The conventional organic dyes are associated with several limitations like photobleaching, limited possibility of multicolour imaging, autofluorescence and dependence of emission on chemical environment [50]. The photobleaching can be reduced by the encapsulation of the dye inside a rigid matrix and autofluorescence can be reduced to a greater extent by the usage of NIR emitting dyes instead of conventional dyes [58].

Quantum dots (QDs) provide a class of biomarkers that could overcome the limitations of organic dyes. The emission spectra of QDs can be tuned by changing the size as well as composition. QDs in general, are resistant to metabolic degradation and privileged by high extinction coefficients as well as conjugation ability. The broad excitation and narrow emission spectra of QDs are favourable for bioimaging, since such spectral behaviour effectively reduces the spectral overlap. The broad excitation spectrum implies the usage of single excitation wavelength to excite QDs of different colours. This is an important advantage of QDs over organic dyes. However, in most of the cases the bare QDs are susceptible to photooxidation. This can be prevented by capping the QDs with a protective shell [59]. The potential toxicity of QDs limit their biological applications [60].

In contrast to QDs, gold nanoclusters (Au NCs) exhibit low toxicity, good water solubility, high biocompatibility, ultra fine size, and tunable photostability. They can be easily fabricated and surface functionalised. Such properties make them promising for bioimaging applications [47]. When the metal NP size approaches below 2 nm, the continuous band structures break up into discrete energy levels and exhibit an electronic transition, which leads to photoluminescence. The fluorescence of Au NCs originates as a result of electronic excitation from the valence band (filled $5d^{10}$) to the conduction band ($6sp^1$) by HOMO-LUMO interband transition.

The lanthanide ion doped NPs have an edge over quantum dots (QDs) by virtue of their stable luminescence, sharp emission peaks with narrow band width, lack of blinking and biocompatibility. The optical properties of the trivalent lanthanide ions, Ln(III) are characteristics of their electronic energy levels, generated by the electronic configurations $[Xe]4f^n$ (n=0–14). The transitions in Ln(III) ions range over UV, visible and near-infrared (NIR) regions [61]. The three types of transitions that are involved in Ln(III) ions are ligand to metal charge transition (L-MCT), 4f-5d and intra configurational 4f-4f. Among these the last transition is more relevant for the bioapplications [62]. The 4f-4f transitions in Ln(III) ions may be magnetic dipole transitions or electric dipole transitions [63, 64]. 4f-5d transitions are highly energetic and

broader than 4f-4f transitions and are commonly observed in trivalent ions of Ce, Pr and Tb [65]. In Ln(III) complexes, the forbidden f-f transitions leads to weak intrinsic luminescence due to low molar absorptivity [63, 66]. Thus intense light source like lasers are required to populate the excited states of Ln(III) ions in complexes, which makes them impractical for majority of biological imaging [67]. However, the attachment of a light-harvesting antenna ligand can circumvent this problem by sensitizing the Ln(III) ions through the so called antenna effect [68].

Downconversion and upconversion luminescence

Based on the mechanism of luminescence, luminescent nanomaterials are classified into upconversion NPs (UCNPs) and downconversion NPs (DCNPs) [69]. Downconversion (DC) is a non-linear optical phenomenon in which a high energy photon is absorbed followed by the emission of two low energy photons. The high energy photon is generally absorbed from the UV region and the emission is in the visible or IR region. A number of host materials including hydroxyapatite have been synthesized with DC luminescence [65]. It can be generalized that trivalent Eu, Dy, Tb, Sm and Nd are used in DC. Eu and Sm produces red emission, Dy causes blue or yellow emission, Tb provides green emission and Nd causes NIR emissions [70, 71]. A detailed mechanism of DC luminescence is appeared in [72].

The term upconversion (UC) relates to an effect by which low energy NIR radiation is converted to high energy visible light by sequential multi photon NIR absorption and subsequent emission of shorter wave luminescence [73]. In lanthanide base UCNPs, Ln(III) ions are dispersed in a dielectric host material with a dimension less than 100 nm. The Ln(III) ion dopant produces luminescence upon excitation [74]. There are five basic mechanisms for UC. They are (a) excited state absorption (ESA) (b) energy transfer upconversion (ETU) (c) co-operative sensitization upconversion (CSU) (d) cross relaxation (CR) and (e) photon avalanche (PA). Complete descriptions of all theUC mechanistic pathways are appeared in [46, 74–76]. The major challenge associated with the UCNPs is to increase their UC efficiency. Selection of host materials with low phonon energy is a best method for achieving high UC efficiency. This is because systems with low phonon energy can minimise non-radiative loss and enhance radiative emission. Lanthanide fluorides are often selected as host materials for developing UCNPs because of their low phonon energy and chemical stability [65]. Several methods are employed to enhance the efficiency of UCNPs. They involve process like plasmonic enhancement of upconversion, tailoring of local crystal field around Ln(III), nanoscopic control of energy transfer process, incorporation of metal shell etc.[65, 74].

Types of luminescent HAp NPs

We shall discuss various luminescent HAp NPs that have been fabricated and explored for bioimaging applications. Among various fluorescent labels described earlier, lanthanide ion dopants and organic dyes are mainly used as fluorescent labels in the fabrication of luminescent HAp NPs. Figure 3 shows various fluorescent labels used in the fabrication of luminescent HAp NPs. It has been observed that most of the luminescent HAp NPs are based on Eu-dopant as a fluorescent label and hence it is more convenient to consider them separately.

Eu-doped luminescent HAp NPs

Among various luminescent Ln(III)-complexes, Eu(III) and Tb(III) have received a great deal of interest because of several desirable factors like biologically appropriate emission in the visible region, long luminescent life time and less sensitivity to quenching by singlet oxygen [77]. Luminescent 4f-4f transitions of Eu(III) and Tb(III) ions leads to the emission of red and green light respectively. Among the Ln(III) ions, the Eu(III) ion is considered to be the most useful spectroscopic probe in view of its non-degenerate emissive state of $^5D_0$ and the ground state of $^7F_0$. Eu(III) is the most widely used lanthanide ion to fabricate luminescent HAp.

Eu(III) doped HAp NPs have been prepared by common synthetic strategies like co-precipitation method [78–81], hydrothermal synthesis [82], thermal decomposition method [83] and microwave assisted hydrothermal method [84]. In each case, the nanocrystals exhibit different morphology and different aspect ratio (length to diameter ratio). They however, show nanometric dimensions around 100 nm. In most of the cases, the luminescence is due to the $^5D_0$-^7F_J (J=0, 1, 2, 3, 4) transitions of Eu(III). The luminescence intensity keeps on increasing with concentration of the dopant up to certain level and above which concentration quenching is observed. Thus the concentration of Eu(III) at which high luminescence intensity is observed can be optimised. The $^5D_0$-$^7F_2$ transition (red emission) of Eu(III) ion is of an electric - dipole (ED) nature and very sensitive to its site symmetry. However, $^5D_0$- $^7F_1$ transition (orange emission) is of a magnetic - dipole (MD) nature and insensitive to site symmetry [85]. It has been observed that the ratio of the red emission to the orange emission shows size dependence [81]. Eu(II) and Eu(III) doped calcium deficient hydroxyapatite (Ca-D HAp) NPs were also fabricated by co-precipitation[86] and combustion synthesis [87]. The emission spectra shows a broad peak with centre at 450 nm corresponds to $4f^6\ 5d^1 \rightarrow 4f^7$ transition of Eu(II) ion and sharp peaks due to $^5D_0$-^7F_J of Eu(III) [86]. It has been observed that the luminescent properties are different in Eu(III) doped HAp and calcium deficient HAp (Ca-D HAp), even though they possess similar crystallite size [87]. Eu(III) doped fluorapatite (FAp) NPs were synthesized by hydrothermal method [88].

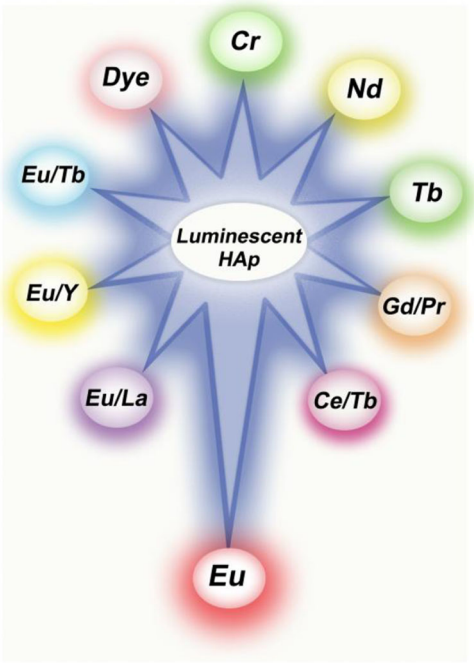

Fig. 3 Fluorescent labels in luminescent HAp NPs

They exhibit spherical morphology and Eu(III) ions are centred at FAp lattice. Arginine modified Eu-doped HAp NPs are obtained by hydrothermal synthesis [89]. They exhibit no cytotoxicity in human epithelial cells and endothelial cells. Eu-doped HAp NPs embedded in PMMA matrix [90] have been reported.

In the mentioned systems the researchers explored the luminescent properties, biocompatibility as well as other characteristics of nanometric HAp. But biomedical applications including bioimaging have not been focused or explored. However several reports on bioimaging and drug delivery applications of Eu-doped luminescent HAp NPs are available. The Eu-doped HAp based nanomaterials for use in luminescent bioimaging as well as drug delivery are detailed in Table 3.

From Fig. 3 it is clear that several dopants can make HAp NPs luminescent and most of such dopants are lanthanide ions. In addition to Eu-doped HAp, luminescent HAp NPs can also be derived by doping with Tb, Nd, Cr, organic dyes, Eu/Tb, Eu /La, Eu and Y, $CePO_4$ and Tb and finally Gd and Pr. Most of such HAp NPs are explored for bioimaging and related applications. The luminescent HAp NPs with dopants other than Eu and having biomedical applications are detailed in Table 4.

The Tb-doped HAp NPs [103, 104] exhibit green emission and it has been observed that Tb-doped FAp shows more green fluorescence intensity than Tb-doped HAp [103]. This is probably due to the presence of OH^- quenchers in HAp. In Tb-doped HAp, the emission is observed due to the $^5D_4$-$^7F_{3–6}$ transition of Tb(III) [105]. Cr doped HAp NPs have been fabricated and the luminescence is due to the $^4T_1(F)\rightarrow{}^4A_2(F)$ transitions of the Cr ions[112]. Gd and Pr co-doped HAp NPs have been prepared by co-precipitation method. Here the PL emission shows a narrow band at 313 nm, which is due to the $^6P_{7/2} \rightarrow {}^8S_{7/2}$ transition in Gd^{3+} ion. The intensity of this emission can be enhanced by Pr^{3+} doping [118]. It should be noted that strontium hydroxyapatite ($Sr_5(PO_4)_3OH$, SrHAp) in nanometric dimensions also exhibit luminescence (blue emission) [119, 120]. This arise from $CO_2^{\cdot-}$ radical impurities in the crystal lattice. These systems are not yet explored for the bioimaging applications.

Lanthanide doped upconversion nanoparticles are highly useful and widely accepted imaging probes [121]. Such probes can be incorporated into HAp to yield upconversion nanosystems for bioimaging. HAp nanorods functionalised with YVO_4:Yb^{3+}, Er^{3+} upconverting NPs have been synthesized by the sol–gel synthesis and the obtained system found potential application in bioimaging [122]. Flurophore doped calcium phosphate NPs were prepared and employed in non-toxic biomedical applications including bioimaging [123].

Magnetic HAp nanoparticles

The magnetic HAp NPs can be fabricated by the incorporation of paramagnetic, ferromagnetic or super paramagnetic labels into the nano matrix of HAp. The commonly used paramagnetic labels are trivalent lanthanide ions or transition metal ions. Ferromagnetic and superparamagnetic labels include Fe(II), Fe(III), magnetite (Fe_3O_4) or maghemite (γ-Fe_2O_3) [124]. The paramagnetism in trivalent lanthanide ions and transition metal ions aroused from the unpaired electrons of f-orbitals of anti penultimate shell and d-orbitals of penultimate shell respectively. The common paramagnetic labels and related magnetic moments are shown in Table 5.

The magnetic nanoparticles are characterised by magnetisation (M), coercivity (H_c) and magnetocrystalline anisotropy constant (K). The term magnetisation represents the extent to which the substance is magnetised under a given magnetic field. The highest value of M is known as saturation magnetisation (M_s). Coercivity is the strength of external magnetic field required to make the magnetisation of a nanoparticle zero. Magnetocrystalline anisotropy constant reflects the energy required to change the direction of magnetisation from easy to hard axis [125]. Iron oxide nanoparticles exhibit the phenomenon of superparamagnetism, in which NPs have zero coercivity and retentivity [126]. The zero coercivity of superparamagnetic iron oxide nanoparticles (SPION) is a favourable feature for biomedical applications. This is because zero residual magnetisation prevents their coagulation and helps in sustaining a long period of circulation in the body [127]. Magnetic NPs including HAp based magnetic nanoparticles have been synthesized, modified and explored for biomedical applications including bioimaging [128–130].

Table 3 Representative hydroxyapatite based nanomaterials for use in luminescent bioimaging (Eu-dopant as fluorescent label) and drug delivery

Nanosystem/ Dopant	Properties	Applications	Synthesis	Ref.
Eu-doped HAp	NPs exhibit nanometric dimensions and mesoporous structure	Fluorescence imaging of HEK293 cells and further bioimaging as well as drug delivery applications	Co-precipitation method	[91]
Eu-doped HAp	The particle size ranges between 30 and 100 nm and the emission decay depends on the percentage of Eu^{3+}	Can be explored in optical imaging	Co-precipitation method	[92]
Eu-doped HAp	The luminescence is enhanced by the thermal treatment and increase in Eu^{3+} concentration; particle diameter 20–40 nm	Promising nanoprobes for fluorescent labelling	Ultrasound assisted precipitation method	[93]
Eu-doped HAp	The average particle size is 13 nm; luminescent intensity increases with increase in Eu^{3+} concentration up to 12 %; concentration quenching is observed above 15 %	The NPs can be used for the imaging of the tumour cells and living cells and also for the targeted drug delivery	Liquid phase laser ablation method	[94]
Eu-doped HAp nanowhiskers	Nanowhiskers with an approximate diameter of 80 nm.	Can be used in bioimaging	Microwave assisted solution combustion synthesis	[95]
Luminescent and mesoporous Eu-doped HAp	Rod-like morphology; particle size of 20–40 nm in width and 100–200 nm in length	Can be used as luminescent drug carrier and in bioimaging	Cationic surfactant template assisted synthesis	[96]
Arginine functionalised Eu- doped HAp	Addition of arginine to HAp NPs causes the diminishing of NP size; can be internalised into the cytoplasm and perinuclear of human lung epithelial cells	Found potential application in bioimaging	Hydrothermal synthesis	[97]
Eu-doped fluorine-substituted HAp	Rod-like morphology; aspect ratios dropped with increase in pH of the solution; luminescence intensity increased with increase in substitution of OH^- with F^-	Applicable for cell labelling of cells like HeLa cells or tracing them in situ	Hydrothermal method	[98]
Eu-doped HAp and fluoroapatite functionalized with poly (acrylic acid)	Spindle like morphology; showed the typical red luminescence of Eu^{3+}, which is more efficient for the fluoroapatite NPs than for the HAp.	Can be used in biomedical imaging	Microwave assisted hydrothermal synthesis	[99]
Eu-doped apatitic calcium phosphate	Calcium-deficient and rich in hydrogen phosphate ions; nanometric sized crystallites; internalizable by human pancreatic cells	Can be used in bioimaging	Wet chemical synthesis	[100]
Eu-doped amorphous calcium phosphate porous nanospheres	Most intense luminescence peak (at 612 nm) is observed at 5 mol% Eu^{3+}; particle diameters in the range of 10–60 nm	Can be used as luminescent drug carriers and for bioimaging	Microwave assisted solvothermal synthesis	[101]
SiO_2/calcium phosphate: Eu^{3+} core-shell NPs	SiO_2 cores with a particle diameter of 46 nm coated with ~ 6-nm-thick Eu^{3+} - doped calcium phosphate shell	Potential application in bioimaging	Sol–gel route followed by annealing	[102]

Table 4 Representative hydroxyapatite based nanomaterials for use in luminescent bioimaging (Eu and /or other dopant as fluorescent label) and drug delivery

Nanosystem/ Dopant	Properties	Applications	Synthesis	Ref.
Tb-doped fluorapatite (FAp) and HAp	Uniform slender morphology; doping of Tb^{3+} ions promote the preferential growth of apatite along the *c*-axis (002) direction; FAp shows more green fluorescence intensity than HAp	Used in cell imaging as well as the tracking of cells	Hydrothermal synthesis	[103]
Tb-doped HAp	20 nm-sized HAp nanoparticles; partially doped with a small amount of Tb; excellent biocompatibility	Nano inorganic imaging probe for living cells	Co-precipitation method	[104]
Ln (Eu^{3+}, Tb^{3+}) doped HAp	Rod-like morphology; well dispersed and non-aggregated size distribution; photoluminescence of Eu^{3+} and Tb^{3+} can be tuned by altering the solvothermal temperature and the dopant concentration	Used as luminescent drug carriers and can be explored for bioimaging	Solvothermal synthesis	[105]
Fluoridated HAp:Ln^{3+} (Ln = Eu or Tb) NPs	Rod like morphology; diameter less than 20 nm	Cell imaging applications	hydrophobic/hydrophilic transformation with surfactants (Pluronic F127)	[106]
Ln^{3+} (Eu, Tb) doped apatitic calcium phosphate	Monodisperse nanorods of 12 nm in average length and around 4 nm in width	Can be used as a fluorescent probe for biomedical imaging	Wet chemical synthesis	[107]
PEGylated hydrophobic fluoridated FAp:Ln^{3+} (Ln = Eu or Tb)	Morphology and fluorescent properties of the FAp nanorods are not significantly changed by the PEGylation; the nanorods are stable in aqueous solution.	The PEGylated NPs are highly biocompatible and can be used in cellular imaging	Reversible addition-fragmentation chain transfer (RAFT) polymerization	[108]
Eu^{3+} and Y^{3+} co-doped HAp/ silica core shell nanorods	Nanorods are 50–100 nm in length and 30 nm in width; Y^{3+} doping, hydrothermal treatment and TEOS coating increases the emission intensity	Can be used for biomedical applications including bioimaging	Co-precipitation method	[109]
Lanthanide-doped HAp (Eu: HA and Eu–La: HA)	Sphere-like morphology; well dispersed and non-aggregated size; PL emission intensity of Eu^{3+} can be tuned by importing La^{3+} ions into Eu: HAp and altering the concentration of Eu^{3+}	Can be explored for bioimaging applications	microemulsion mediated hydrothermal process	[110]
$CePO_4$:Tb doped HAp	Needle like nanoparticles of 50–100 nm length and 5–10 nm width	Can act as redox luminescent switch as well as bioimaging probes	Co-deposition of $Na_2HPO_4.12H_2O$ and $CaCl_2$ in the presence of $CePO_4$:Tb at RT	[111]
Cr^{3+}-doped HAp	The average particle size ranges from 40 to 100 nm; PL emission is associated to the $^4T_1(F) \rightarrow {}^4A_2(F)$ transitions of the Cr ions.	The luminescent property can be explored in bioimaging / biosensing	Co-precipitation method	[112]
Nd -doped HAp	High aspect ratio; needle-like morphology; the emission from Nd^{3+} is caused by 4f electrons that are shielded from the surrounding by 5 s and 5p shells	promising as multifunctional drug delivery systems for simultaneous targeted drug delivery and NIR fluorescence imaging	Co-precipitation method	[113]
Dye (FITC) functionalized HAp	Needle like morphology with 50–100 nm length; internalizable by HeLA cells	Can be explored for cellular imaging, drug delivery and drug release	Template assisted synthesis, using SiO_2	[114]
Methylene blue (MB) dye encapsulated HAp/silica core-shell structures	Large size of about 100 nm; dual luminescence in the PL spectra due to the presence of monomer and dimmers of MB	Can be explored for bioimaging and or theranostic applications	Wet-chemical precipitation technique	[115]
Organic dyes(Cascade Blue, SAB, fluorescein sodium salt, rhodamine WT, and Cy3 amidite) encapsulated calcium phosphate	organically doped calcium phosphate spherical nanoparticles; 20–30 nm in diameter	Promising luminescence and capability to bear organic molecules makes the system adaptable for drug deliver as well as imaging applications.	Reverse microemulsion procedure	[116]
Calcium phosphate nanoparticles in which molecules of NIR emitting fluorophore, indocyanine green (ICG), are embedded	Colloidal particles with average diameter 16 nm; colloidally stable in physiological solutions (PBS) with carboxylate or PEG surface functionality	In-vivo imaging of human breast cancer	Reverse micro emulsion synthesis	[117]

Table 5 Magnetic moment paramagnetic labels

Paramagentic ion label	Electronic arrangement	Unpaired electrons	Magnetic moment(μ_B)
Mn(II)	$3d^5$	5	5.91(spin only moment)
Co(II)	$3d^7$	3	3.87(spin only moment)
Gd (III)	$4f^7$	7	7.94(effective moment)
Dy(III)	$4f^9$	5	10.6(effective moment)
Ho(III)	$4f^{10}$	4	10.64(effective moment)
Tm(III)	$4f^{12}$	2	7.56(effective moment)

Most of the magnetic HAp NPs are based on Fe(II), Fe(III) or iron oxides. However magnetic HAp NPs based on other dopants are also reported. Different magnetic HAp NPs categorised based on the magnetic labels are shown in Fig. 4. The magnetic HAp NPs include eight different categories such as (i) Fe-doped, (ii) Fe and Pt co-doped, (iii) Nd and Gd co-doped (iv)Co ferrite doped, (v) iron oxide doped, (vi) Mn and Fe doped, (vii) ^{153}Sm and Gd incorporated and (viii) iron oxide, Fe and Cu doped HAp NPs.

Fe-doped HAp nanocrystals with different morphology and different nanometric dimensions have been fabricated by conventional methods like sol–gel synthesis [131], co-precipitation method [132] and ion-exchange method [133]. It has been observed that the particle size decreases as the concentration of iron dopant increases [131]. In this case simultaneous changes in the crystallinity degree, lattice parameters, unit cell volume and the phase composition are also observed. Nd(III) and Gd(III) substituted HAp has been prepared by ion-exchange method [134]. Here the electrical conductivity of HAp is improved because of the high polarizability of Nd(III) and Gd(III). Cobalt ferrite doped ferromagnetic HAp NPs with core-shell structure have been prepared developed by co-precipitation method [135]. Here HAp is in the shell and Coferrite($CoFe_2O_4$) is in the core. Iron oxide (both magnetite and maghemite) incorporated HAp NPs have been prepared by co-precipitation method [136–138]. Mn and Fe incorporated HAp nanocrystals have been prepare by wet chemical method coupled with ion exchange mechanism [139]. Compared with Mn^{2+}ions, Fe^{3+} ions were more active in replacing Ca^{2+} in HAp lattice. The mentioned magnetic HAp NPs are not explored for imaging applications. However, several magnetic HAp NPs have been reported for biomedical applications including bioimaging and drug delivery. They are detailed in Table 6.

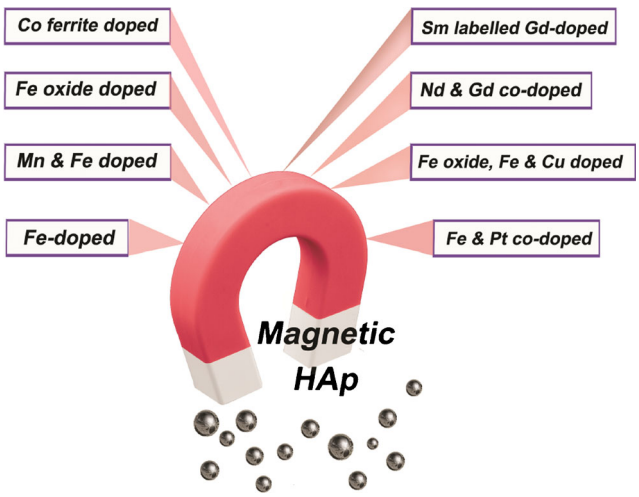

Fig. 4 Types of magnetic HAp NPs

Luminomagnetic HAp NPs

Incorporation of fluorescent and magnetic labels in nanocrystalline HAp enables the formation of luminomagnetic bifunctional HAp NPs. The important advantage of such bifunctional systems is that both magnetism as well as luminescence can be simultaneously explored for biomedical applications. This strategy is very useful in developing bimodal or multimodal imaging probes. Several bifunctional lumino magnetic systems have been fabricated and explored for bimodal or multimodal imaging applications as well as drug delivery (Table 7).

Drug delivery and molecular imaging applications of HAp based nanoprobes

In this section we shall describe the drug delivery and molecular imaging applications of HAp based nanoprobes. It is clear from the preceding sections that luminescent, magnetic and luminomagnetic HAp NPs are explored for various imaging as well as drug delivery applications. For biomedical applications such as drug delivery and bioimaging, it is necessary to target the nanoprobes into relevant biological sites of therapeutic and diagnostic importance.

Targeting of HAp based nanoprobes for drug delivery and bioimaging

Modification of the imaging probes with targeting ligands leads to specific interaction of the probes with the receptors on the target cell. As a result of this specific interaction the imaging probes selectively accumulate at the target site for a long period of time and produces images with high spatial resolution. The imaging probes with targeting moieties can produce high quality images even at low concentration compared to the same nanoparticles without targeting moieties [16]. The targeting moieties may be proteins, carbohydrates, lipids, vitamins or polymers. Such moieties can be conjugated to the nanoprobes using various conjugation methods including host-guest physical interactions [159]. The correct choice of the conjugation method avoids the deterioration of the imaging resolution and ameliorates high quality diagnosis [160].

Table 6 Representative hydroxyapatite based nanomaterials for use in magnetic imaging and drug delivery

Nanosystem/ Dopant	Properties	Applications	Synthesis	Ref.
^{153}Sm labelled Gd- doped HAp	Rod - like morphology with average diameter about 8 nm and length nearly 25 nm; HA:Gd nanorods are well dispersed on the substrate	Used as SPECT/MRI dual imaging probe	Hydrothermal synthesis	[140]
(Fe^{2+}/Fe^{3+})-doped HAp-collagen composite	The morphologies are different in dependence on the synthesis temperature; nanocomposites exhibit superparamagnetic behaviour	Can be explored for in vivo MRI applications	Wet chemical synthesis	[141]
Iron (Fe^{3+} and Fe^{2+}) doped HAp	Needle - like morphology; superparamagnetic; shows higher cell proliferation and osteoblast activity	The NPs can be explored for diagnostic imaging or magnetic drug delivery.	Co-precipitation method	[142]
HAp/ γ-Fe_2O_3 hybrid nanostructure	Feather-like or spherical morphology; γ-Fe_2O_3 NPs dispersed within the HAp matrix; superparamagnetic feature; can be controlled by the external magnetic field	Can be explored for targeted drug delivery	Co-precipitation method	[143]
Mn and Fe incorporated core/shell type HAp	The core being formed by the ferrites and the shell by the hydroxyapatite; Mn^{2+} ions are substituted in Ca(1) site of HAp.	Can be explored for hyperthermia applications for the treatment of bone cancer as well as for MRI contrast	Co-precipitation method	[144]
Iron doped HAp-Poly lactic acid(PLA) composite	Fe-HAp NCs have needle-like morphology and nanometric dimensions in the range of 5–20 nm in width and 50–80 nm in length	Potential use as building blocks for the preparation of scaffolds for hard tissue regeneration and can be used in nanomedical applications including MRI	Fe-HAp by wet chemical synthesis and Fe-HAp coated PLA micro-nanospheres by pickering emulsion method	[145]
Iron (Fe^{3+} and Fe^{2+}) doped HAp	NPs have Ca/P ratio 1.67 and Fe^{3+}/Fe^{2+} ratio around 3; exhibit superparamagnetic behaviour	Can be used as anti-cancer agents based on hyperthermia	Wet chemical synthesis based on neutralization	[146]
Fe_3O_4, Fe and Cu doped HAp/glass composite	Porous nano structure; magnetic properties depend mainly on composition and nature of additives; Fe_3O_4 doped sample exhibit strong ferromagnetism.	Can be used for targeted drug delivery and can be explored for MRI	Wet chemical synthesis	[147]
Fe^{2+} and Pt^{2+} doped HAp	Pt and Fe contents were 3.69 wt% and 12.20 wt%, respectively; exhibit ferromagnetic behaviour at room temperature	Can be used as chemo-hyperthermia dual modality for the treatment of lung cancer	Co-precipitation method	[148]
Iron doped HAp	Particles dimensions are in the nano regime; exhibit considerable magnetic behaviour.	Can be used as L-tyrosine sensor	Microwave irradiation method	[149]
Iron doped HAp	Rod- like structure with an average particle size of 75 nm; size of doped HAp is less than undoped sample; Fe^{3+} doping decreases the particle size and increases the hardness; doped sample exhibit superparamagnetism	Used as nanoprobes for drug releasing	Combination of hydrothermal and microwave techniques	[150]

Table 7 Representative hydroxyapatite based nanomaterials for use in bimodal/ trimodal imaging and drug delivery

Nanosystem/Dopant	Properties	Applications	Synthesis	Ref.
Eu^{3+} and Gd^{3+} doped HAp	Average size 30 nm; hexagonal crystal structure; Eu^{3+} offered luminescence and Gd^{3+} offered paramagnetism.	Used as tri-modal contrast agents in imaging such as MRI, X-ray imaging and NIR fluorescence imaging	Surfactant free aq.wet chemical synthesis	[151]
$Tb^{3+/}Gd^{3+}$ dual-doped multifunctional HAp	Sphere-like morphology; particle sizes ranging from 40 to100 nm; luminescent and paramagnetic behaviour; PL emission intensity increases with increasing concentration of Gd^{3+} ions; magnetization level increases with the concentration of Gd^{3+} ions	Can be explored for bimodal imaging applications	Co-precipitation method	[152]
Aptamer caped Gd-doped luminescent and mesoporous SrHAp	NPs have average length of 100–120 nm, diameter of about 20 nm, and aspect ratio of 5.0	Used in the fluorescence imaging (MCF-7 cells) and as T1 contrast agent	Wet chemical synthesis	[153]
Eu^{3+} and Gd^{3+} dual doped HAp	Nanorods show nanometric dimensions; photoluminescent and magnetic multi functions are realized by the dual-doping with Eu^{3+} and Gd^{3+}; PL intensity of can be adjusted by varying Eu^{3+} and Gd^{3+} concentrations	Can be used as a multiple-model imaging agent MRI, PL imaging and CT imaging	Microwave assisted synthesis	[154]
Calcium phosphate doped with both indocyanine green (ICG) and Gd, and labeled with 99 m-Technetium-methylene diphosphonate (^{99m}Tc-MDP)	NPs show nanometric dimensions; doping with ICG and Gd^{3+} aided NIR and MR contrast; surface tagging with ^{99m}Tc resulted radioactive emission suitable for nuclear imaging.	Can be used as tri-modal contrast agent for nuclear, magnetic and near-infrared imaging in vivo	Wet chemical synthesis	[155]
Eu^{3+} and Gd^{3+} dual-doped calcium phosphate nanospheres	Shows strong NIR emission at 700 nm; the PL intensity can be adjusted by varying Eu^{3+} and Gd^{3+} concentrations; shows paramagnetism	Can be used as multifunctional drug delivery systems and tissue engineering scaffolds with bioimaging guidance	Wet chemical synthesis	[156]
HAp composite functionalized with up-conversion (UC) luminescent and magnetic Na(Y/Gd)F4:Yb^{3+}, Er^{3+}nanocrystals	Contrast brightening is enhanced at increased concentrations of Gd^{3+}	Have potential applications in drug storage/release and as bimodal contrast agents in MRI /UC luminescence imaging	Electro spinning method	[157]
HAp NPs dually doped with paramagnetic and fluorescent label.	Magnetism is endowed by Ho(III)ion and luminescence is offered by organic dye, FITC	Used in the in vitro cell imaging of HeLa cells and find potential application as T2 MRI contrast agent	Wet chemical synthesis without surfactants.	[158]

Figure 5 schematically represents the targeting of HAp based nanoprobes for bioimaging and drug delivery.

HAp nanoprobes can be conjugated with different targeting moieties to enable targeted cellular imaging. Amino acids like arginine [97], proteins like albumin [105], vitamins like folic acid [151, 158] etc. can be used as targeting moieties. The targeting moieties can be anchored through surface coating of the HAp NPs with poly acrylic acid (PAA), poly lactic acid (PLA), poly ethylene glycol (PEG) or poly ethylene imine (PEI). It is a well established fact that folic acid conjugated HAp NPs produces targeted imaging through interaction with the folate receptors over expressed in many cancer cells. The folate receptor based targeted drug delivery is highly promising in cancer therapy.

Drug delivery applications

Precise drug release into highly specified targets involves miniaturizing the delivery systems to become much smaller than their targets. These minute drug delivery systems can be realized through the advances in the nano biotechnology. A wide variety of nanosystems have been developed for targeted drug delivery applications. Biocompatible and biodegradable HAp NPs mesoporous structures have great potential in drug delivery systems. HAp NPs are used as drug delivery systems for various classes of drugs, protein drugs, enzymes, ibuprofen, antibiotics, 5- fluorouracil and Adriamycin. Folic acid modified poly ethylene glycol functionalised HAp NPs are used in the paclitaxel drug delivery [161]. Hollow mesoporous HAp NPs exhibit enhanced drug loading efficiency and pH responsive release for the drug doxorubicin (DOX) [162]. HAp microspheres act as vehicles for sustained delivery of small molecular drugs like doxycycline hydrochloride [163]. Thus the usage of HAp NPs for drug delivery is promising. In this section we shall consider the drug delivery applications of luminescent, magnetic and luminomagnetic HAp NPs.

Luminescent Nd-doped HAp NPs complexed with cyclodextrin were prepared by co-precipitation method and successfully demonstrated in drug delivery applications. The said NIR emitting NPs exhibit needle-like morphology and the in vitro loading and releasing studies were performed by using DOX as a model drug [113]. Organic dyes incorporated luminescent calcium phosphate NPs were used in the in vitro delivery of the chemotherapeutic drug, ceramide to human vascular cells [116]. Eu-doped amorphous calcium phosphate NPs were used as luminescent drug carriers for the drug ibuprofen [101]. Magnetic HAp NPs doped with varying levels of Fe^{3+} was synthesized by hydrothermal and microwave assisted method. These NPs showed sustained release for the drugs amoxicillin and 5- fluorouracil at lowest concentration of Fe^{3+} [150]. Fe_3O_4 doped ferromagnetic HAp NPs found potential application in targeted delivery of drugs [147].

Several multifunctional HAp NPs with luminescence and magnetism are also demonstrated for drug delivery applications. Sm^{3+} and Fe^{3+} co-doped magnetic and luminescent mesoporous HAp nanocrystals were prepared by template assisted synthesis. The nanospindles thus obtained have a large pore volume, high surface area and high drug payload ratio which made them highly suitable for drug delivery [164]. Eu^{3+} and Gd^{3+} dual doped luminomagnetic HAp nanorods were prepared by microwave assisted synthesis and the obtained nanorods showed high drug adsorption capacity as well as sustained drug release [154]. Porous HAp composite functionalised with upconversion luminescent and magnetic nanocrystals were fabricated by electrospinning method. The said nanocomposite found potential application as a drug carrier [157]. Aptamer caped multifunctional strontium substituted HAp NPs were demonstrated for cancer cell responsive drug delivery applications [153]. Sustained drug releasing capability of Eu^{3+} and Gd^{3+} dual doped multifunctional calcium phosphate nanospheres were demonstrated by using ibuprofen as a model drug [156]. The difficulties associated with the preparation of stable nanoscaled HAp NPs with and without porous structures limit the application of HAp NPs in drug delivery and other biomedical applications.

Molecular imaging applications

Luminescent HAp NPs are employed in optical imaging including NIR and upconversion luminescence imaging, by virtue of their luminescence. Magnetic HAp NPs are good candidates for MRI applications. Luminomagnetic systems are

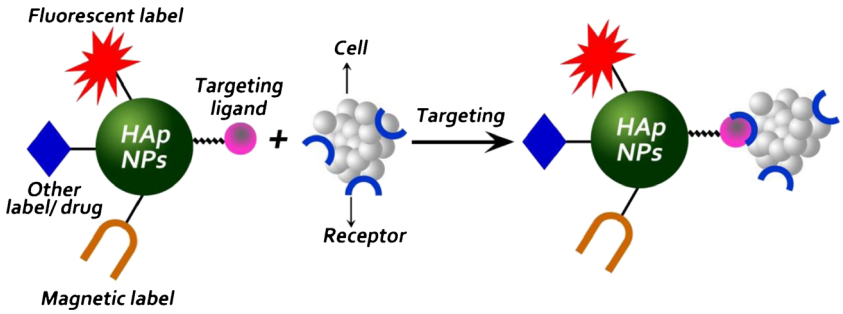

Fig. 5 Schematic representation of targeting of HAp based nanoprobes for bioimaging and drug delivery

useful in bimodal or multimodal imaging by making use of their functional properties. Thus the imaging capability HAp based nanoprobes depends on the nature of the dopants or attaching moieties as reporters for bioimaging. Figure 6 represents the consolidation of imaging applications of HAp based nanoprobes.

Optical imaging using luminescent HAp NPs

The HAp NPs with luminescent properties can be used as imaging probes in luminescence imaging. This imaging may be simple fluorescence imaging, NIR imaging or UC luminescence imaging. It has been observed that a wide variety of cancer cells can be imaged using luminescent HAp NPs as optical imaging probes.

Imaging of human embryonic kidney cells (HEK293) was performed by using mesoporous Eu-doped HAp NPs. The lack of cytotoxic effects of the nanoparticles were analysed by focusing the F-actin filament pattern and heat shock proteins expression in HEK293 cell line [91]. Bel-7402 human liver cancer cells are labelled by using HAp NPs doped with 2 % of Eu^{3+} ion. The NPs are internalized by the cancer cells through endocytosis. The said NPs exhibit a temporally stable luminescence with life time of 19.ms, which enables their function as a promising luminescent imaging probe [93]. The applicability of Eu-doped nanowhiskers in bioimaging is illustrated by confocal microscopic studies of 7F2 cells incubated with the nanowhiskers[95]. Arginine functionalised Eu-doped HAp NPs were successfully employed for optical imaging applications. The biocompatibility and cellular uptake of the said NPs were proved by using human epithelial lung cancer cell line (A549). Arginine functionalisation effectively changes the zeta potential of Eu-HAp NPs to positive values and this enables the specific binding of the NPs to plasmid DNA of cell lines [97]. Eu-doped fluorine substituted HAp NPs are effective imaging probes as proved by fluorescence imaging studies on human cervical cancer (HeLa) cells [98]. Eu-doped HAp NPs were successfully employed in the imaging of human cancerous epithelial pancreatic cells (Capan-1 cell line). Here the confocal microscopic analysis confirmed the internalization of the nanoprobes by the cancer cells, since the luminescent NPs are located around the nucleus of the cell [100].

HAp NPs doped with small amount of Tb is used as a bioimaging probe for cellular imaging. The nanoprobes explore the luminescence of Tb^{3+}, which produce a green emission after excitation with visible light of wavelength 488 nm. The imaging studies were performed on rabbit bone marrow mesenchymal stem cells (MSCs) [104]. Luminescent Nd-doped HAp NPs complexed with cyclodextrin (CD) were used in the drug delivery system as well as for bioimaging. The applicability of the system in bioimaging is confirmed by the cellular uptake and imaging studies performed using C6 glioma cells. The said NPs exhibit a strong NIR emission at 680 nm after excitation at 420 nm. The coating of NPs with CD enables the preferential adsorption of albumin, which implies selective targeting [113].

HAp NPs prepared by using silica template are surface functionalised with FITC dye and are used in the live cell imaging of HeLa cells. The said NPs (THA-FITC) at different concentration (100, 300 and 500 $\mu g.mL^{-1}$) were allowed to interact with HeLa cells for a period of 2 h at 37 °C and confocal fluorescent images are taken (Fig. 7a, b and c). The green fluorescence of FITC, which is proportional to the concentration of THA-FITC NPs, indicates that the NPs are internalized into the cells. Multilabelling laser scanning confocal microscope studies were performed to confirm the intracellular localisation of FITC. For this cytoplasm of HeLa cells was stained with red dye (rhodamine 6G) after incubation of NPs and images were taken for THA-FITC colour and cytoplasmic red colour (Fig. 7c and d). The merged image (Fig. 7f) confirms the intracellular localisation of THA-FITC. The said NPs exhibit low cytotoxicity and are good bioimaging probes [114].

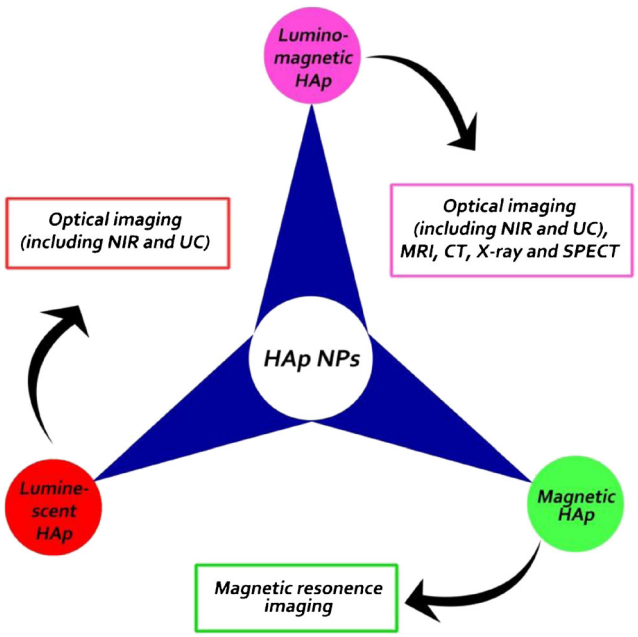

Fig. 6 Molecular imaging applications of HAp based nanoprobes

MR imaging using magnetic HAp NPs

The major role of magnetic HAp NPs in cellular imaging is as the contrast agents (CAs) for MRI. The administration of CAs can improve the applicability of MRI as a valuable diagnostic tool by providing high quality images. The contrast in MR images is generated by the difference in the proton density between tissues and the difference in T1 and T2 relaxation

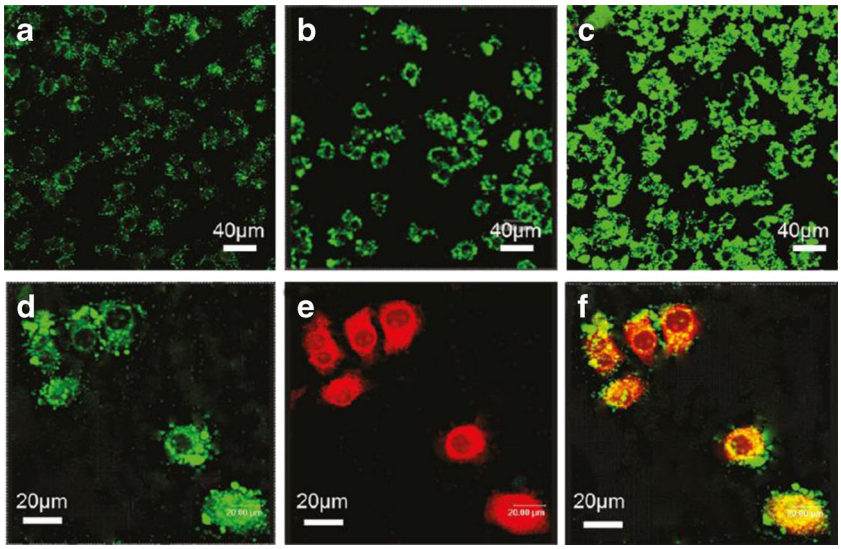

Fig. 7 Confocal fluorescent images of HeLa cells incubated with THA- FITC nanoparticles with concentrations (**a**) 100 μg.mL^{-1} (**b**) 300 μg.mL^{-1} and (**c**) 500 μg.mL^{-1} for 2 h. Multilabelling laser scanning confocal microscope of HeLa cells incubated with THA- FITC nanoparticles with concentration 300 μg.mL^{-1} for 2 h: (**d**) image showing THA-FITC colour only (**e**) image of cytoplasm illuminated with red dye and (**f**) overlaid image of HeLa cells. (Reprinted with permission from ref. [114]. Copyright 2011 American Chemical Society)

times. The CAs can be positive (T1) or negative (T2) based on their capability to produce a brightening or darkening effect on the MR image, respectively. The commonly used CAs are based on Gd (T1 CAs) and Fe (T2 CAs) [49]. Other paramagnetic lanthanide ions (Dy^{3+}, Ho^{3+}, Tb^{3+} and Er^{3+}) are also used in CAs [22, 165]. T1 and T2 CAs have been developed from magnetic HAp NPs and T1 or T2 contrasting activities of those systems depend on the magnetic label used.

Gd doped magnetic HAp nanorods labelled with radioactive species Sm-153 is employed as the dual modal contrast agent for SPECT and MR imaging in vivo. The high magnetic moment possessed by the Gd^{3+} ion is explored in MRI application and γ- emission from Sm-153 is explored in SPECT imaging [140]. The said nanorods (^{153} Sm-HA: Gd) exhibit excellent biocompatibility as revealed by the methyl thiazolyl tetrazolium (MTT) assay and TEM analysis. T1 weighted images and relaxivity of the nanorods were measured using a 3 T MRI scanner. It has been observed that the T1 weighted MRI signal intensity showed a proportionate increase with nanorod concentration and relaxivity parameter (r_1) at 3 T is calculated experimentally as 5.49 s^{-1} $(mM)^{-1}$. For in vivo MR imaging studies, the nanorods at 15 mg/kg were intravenously injected into BALB/c mice (20 g) and anatomical images were taken. Comparison of pre and post-contrast T1weighted images (Fig. 8a and b respectively) revealed the contrast enhancement in organs like liver and spleen, 60 min after injection. The colour map images of the MR signal showed that the region of the liver and spleen appeared blue and green before injection became yellow and red, 60 min after injection (Fig. 8c and d respectively). The MR images clearly depicted that the

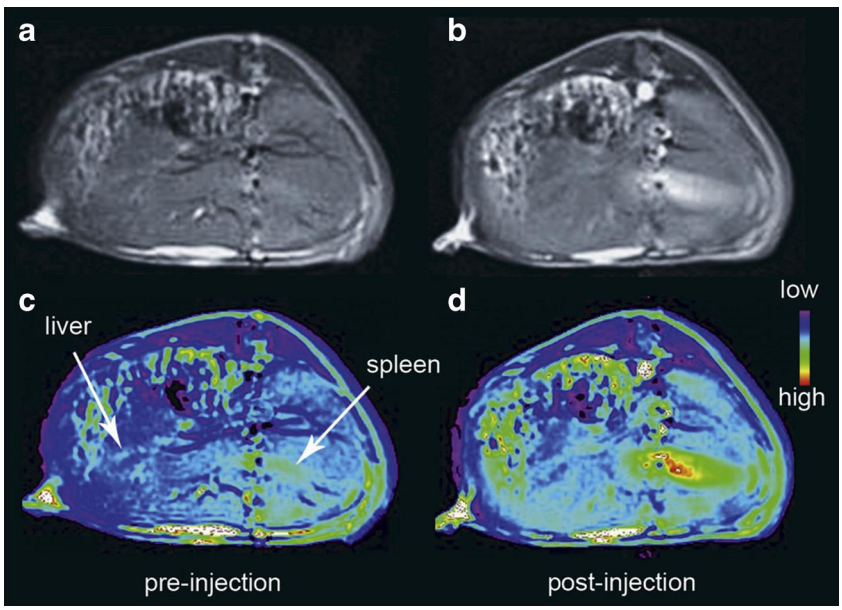

Fig. 8 In vivo MR images (**a**, **b**) and the colour-mapped images (**c**, **d**) of the transversal cross-sectional images of the liver and spleen of mice at pre-injection (**a**, **c**) and at 60 min post injection of HA:Gd nanorods at 15 mg/kg. (Reprinted with permission from ref. [140]. Copyright 2013, Elsevier)

nanorods were readily taken up by the mononuclear phagocytic systems (liver and spleen). The said nanorods are explored for SPECT imaging in vivo. The SPECT images also revealed the uptake of the nanorods by the mononuclear phagocytic systems.

Even though a number of magnetic HAP NPs were developed by doping with different magnetic label ions such as Gd^{3+}, Mn^{2+}, Fe^{2+}, Fe^{3+} etc. only few are found relevant in imaging applications like MRI [142, 145] . This may be probably due to vast availability of other CAs (based on substrates other than HAp) and the wide popularity of T1 CAs (contain Gd) over T2 CAs (contain Fe). A number of the magnetic HAp NPs are explored for other biomedical applications such as targeted drug delivery, magnetic hyperthermia, biosensing and theranostics [143, 144, 146, 148–150]. However, multifunctional HAp NPs are extensively used in multimodality imaging recently.

Multimodal imaging using luminomagnetic HAp NPs

Bifunctional HAp NPs that incorporate luminescence as well as magnetism are highly promising bimodal or multimodal imaging probes. HAp NPs doped with Eu^{3+} and Gd^{3+} is used as a multi modal contrast agent for MRI, X-ray imaging and NIR fluorescence imaging [151]. The said NPs exhibit hexagonal phase with spherical morphology and average particle size is 30 nm. The nanotoxicity analysis of the NPs using different type of cancer cells revealed excellent biocompatibility. The NPs are made suitable for receptor targeted imaging by surface conjugation with folic acid. The T1 MR contrasting activity of the NPs is tested by using 1.5 T clinical MRI system by echo-spin method. The said NPs exhibited high longitudinal realxivity ($r_1 = 12\ s^{-1}\ (mM)^{-1}$) compared to commercial Gd-DTPA complex. The NPs have nearly 80 % X-ray attenuation, which is suitable for X-ray imaging. The Eu^{3+} dopant caused emission at 700 nm, which made the system adaptable for NIR fluorescence imaging. It has been observed that strontium substituted HAp (SHAp) has similar stoichiometry to that of HAp and leads to enhancement of in vitro bioactivity [166]. Aptamer caped Gd-doped luminescent and mesoporous SrHAp NPs were successfully used as dual modal imaging probe for fluorescence imaging and MRI, by virtue of their blue autofluorescence and paramagnetism. The said NPs are also useful for cancer cell responsive drug delivery [153].

Eu^{3+} and Gd^{3+} dual doped HAp nanorods fabricated by microwave assisted synthesis were used as a multiple imaging agent for MRI, photoluminescence (PL) and CT imaging [154]. These biocompatible nanorods are highly useful for drug delivery applications also. In vitro MR imaging studies revealed the potential applicability of the system as a T1 contrast agent. The in vivo PL imaging capability of the nanorods was demonstrated by the subcutaneous injection of the NPs to mice at an optimum concentration of 1 mg. mL^{-1} per animal. The mice were imaged and the obtained images (Fig. 9a and b) clearly depicted the applicability of the nanorods in PL imaging. It has been observed that the solution of the said nanorods produced an intense red emission (Fig. 9c).

For in vivo CT imaging the nanorods were injected to the mice and the mice were imaged by a clinical CT. The in vivo whole body images of the mouse before and after injection at two different injection sites (back of the mouse and buttock of the mouse) produced clearly distinguished CT signals. The signals were obtained because of the attenuation of strong X-rays by the nanorods.

HAp nano composite functionalized with up-conversion (UC) luminescent and magnetic $Na(Y/Gd)F_4$: Yb^{3+},Er^{3+} nanocrystals were used as dual modal imaging probe in MRI and UC luminescence imaging [157]. In vitro MR imaging studies revealed the applicability of the said composite as T1 CAs. Upconversion luminescence microscopy was used to detect the interaction of the MC 3T3-E1 cells with the composite, under NIR laser excitation (980 nm) and the produced images clearly proved the applicability of the said system in

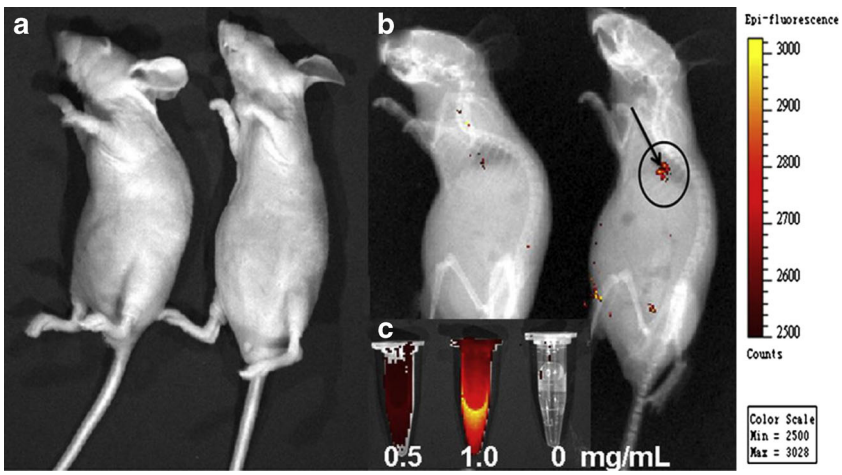

Fig. 9 In vivo PL imaging of the mice after subcutaneous injection (**a**) without Eu^{3+}/Gd^{3+}–HAp nanorods (**b**) with Eu^{3+}/Gd^{3+}–HAp nanorods. (**c**) PL emission images of Eu^{3+}/Gd^{3+}–HAp nanorods at different concentrations. The excitation wavelength was 430 nm. (Reprinted with permission from ref. [154]. Copyright 2011, Elsevier)

UC luminescence imaging. These nanocomposites were also used in drug delivery.

Calcium phosphate doped with indigocyanin green (ICG), Gd and labelled with 99 m Technetium methylene diphosphonate (^{99m}Tc-MDP) is employed as trimodal contrast agent [155]. Here the fluorescence from ICG is explored for NIR imaging, magnetism of Gd utilised for MRI contast and ^{99m}Tc-MDP is exploited for nuclear imaging. Multifunctional Eu^{3+} and Gd^{3+} dual doped calcium phosphate vesicle like nanospheres were employed for multimodal imaging (MRI and NIR luminescence imaging) and sustained drug release [156]. Recently, our research group developed a luminomagnetic HAp nanocrystalline system by doping HAp with paramagnetic label (Ho^{3+}) and fluorescent label (organic dye, FITC). The present system is employed in the fluorescence imaging of cancer cells (HeLa cells) and can be used for MRI contrast by exploring the luminescence of FITC and magnetism of Ho^{3+} respectively [158].

Conclusion

The main objective of this review is to explain state-of-the -art bioimaging applications of HAp based nanoprobes, especially the luminescent and magnetic cellular imaging. HAp nanocrystals can be doped with a variety of dopants like lanthanide ions or can be modified with other substrates and reporter moieties to achieve desirable functional properties. The HAp NPs functionalised in this manner can serve as potential nanoprobes for cellular imaging. Based on the functional properties that explored in bioimaging, HAp NPs are conveniently grouped into luminescent, magnetic and luminomagnetic HAp NPs. The studies on luminescent and magnetic HAp NPs demonstrated their usefulness as potential imaging probes in optical imaging and MRI respectively. The luminomagnetic HAp NPs are good candidates for multimodal imaging, where two or more imaging modes are combined to produce a synergistic effect in diagnostic imaging. The functionalised HAp NPs proved their efficacy as potential nanoprobes for targeted drug delivery. Even though several reports on bioimaging applications of HAp based nanoprobes are available, the exploration of HAp NPs as bioimaging probe is least in comparison with other biomedical applications such as bone tissue engineering, nanomedicine and catalysis. This is probably due to many challenges which hinder the potential applications of HAp NPs as bioimaging probes.

The main challenge is the precise size and morphological control of HAp NPs. Nanometric size with suitable range is essential for the successful application in bioimaging as well as drug delivery. A number of methods are available to synthesise nanocrystalline HAp with different morphologies and any of such method is not completely successful in offering uniform size distribution and morphology. Cell viability studies and toxicity analysis revealed excellent biocompatibility of HAp NPs. However, the effect of functionalised HAp based nanoprobes for long time in vivo is still not known with certainty and need much more systematic investigation. Another challenge is in designing the targeted multimodal imaging system based on HAp. Factors like appropriate choice of targeting moiety, conjugation method of the targeting moiety and selection of surface coating materials for HAp should be considered during the designing such systems. In designing multimodal imaging systems including PET or SPECT, radiation hazards should also be taken into account. The control of pore size in mesoporous HAp NPs has a crucial role in targeted drug delivery applications. More focus is needed to address these challenges to develop highly promising HAp based nanoprobes for imaging as well as drug delivery.

Most of the luminescent and magnetic HAp NPs are fabricated by doping with lanthanide ion labels. Incorporation of other fluorescent labels (organic dyes, gold nanoclusters, UC phosphors etc.) and different magnetic labels (transition metal ions) can enable the design and fabrication novel luminescent as well as magnetic HAp nanoprobes. Derivatives of HAp, like fluorine or strontium substituted HAp can also be employed for the fabrication of bioimaging as well as drug delivery nanoprobes in future.

Acknowledgments The authors would like to acknowledge University Grant Commission (UGC) New Delhi, for providing financial assistance through the Teacher Fellowship under Faculty Improvement Programme (FIP) and the Head, Department of Chemistry, University of Kerala (Kariavattom Campus), Trivandrum.

References

1. Hui J, Wang X (2014) Hydroxyapatite nanocrystals: colloidal chemistry, assembly and their biological applications. Inorg Chem Front 1:215–225
2. Meyers MA, Chen PY, Lin AYM, Seki Y (2008) Biological materials: structure and mechanical properties. Prog Mater Sci 53:1–206
3. Palmer LC, Newcomb CJ, Kaltz SR, Spoerke ED, Stupp SI (2008) Biomimetic systems for hydroxyapatite mineralization inspired by bone and enamel. Chem Rev 108:4754–4783
4. Stigter M, Groot K, Layrolle P (2002) Incorporation of tobramycin into biomimetic hydroxyapatite coating on titanium. Biomaterials 23:4143–4153
5. Fox K, Tran PA, Tran N (2012) Recent advances in research applications of nanophase hydroxyapatite. Chem Phys Chem 13: 2495–2506
6. Lafisco M, Delgado-Lopez JM, Varoni EM, Tampieri A, Rimondini L, Gomez-Morales J, Prat M (2013) Cell surface receptor targeted biomimetic apatite nanocrystals for cancer therapy. Small 25:3834–3844
7. Xu J, White T, Li P, He C, Han Y-F (2010) Hydroxyapatite foam as a catalyst for formaldehyde combustion at room temperature. J Am Chem Soc 132:13172–13173

8. Liu TY, Chen SY, Liu DM, Liou SC (2005) On the study of BSA-loaded calcium-deficient hydroxyapatite nano-carriers for controlled drug delivery. J Control Release 107:112–121
9. Uskovic V, Uskovic DP (2011) Nanosized hydroxyapatite and other calcium phosphates: chemistry of formation and application as drug and gene delivery agents. J Biomed Mater Res B 96B: 152–191
10. Luo Y, Ling Y, Guo W, Pang J, Liu W, Fang Y, Wen X, Wei K, Gao X (2010) Docetaxel loaded oleic acid-coated hydroxyapatite nanoparticles enhance the docetaxel-induced apoptosis through activation of caspase-2 in androgen independent prostate cancer cells. J Control Release 147:278–288
11. Hou C H, Hou S M, Hsueh Y S, Lin J, Wu H C, Lin F H The in vivo performance of biomagnetic hydroxyapatite nanoparticles in cancer hyperthermia therapy. Biomaterials 30:3956–3960
12. Li J, Yin Y, Yao F, Zhang L, Yao K (2008) Effect of nano-and micro-hydroxyapatite/chitosan-gelatin network film on human gastric cancer cells. Mater Lett 62:3220–3223
13. Nazari AG, Tahari A, Moztarzadeh M, Mozafari M, Bahroloom ME (2011) Ion exchange behaviour of silver-doped apatite micro and nanoparticles as antibacterial biomaterial. Micro Nano Lett 6: 713–717
14. Radovanovic Z, Jokic B, Veljovic D, Dimitrijevic S, Kojic V, Petrovic R, Janackovic D (2014) Antimicrobial activity and biocompatibility of Ag^{+} - and Cu^{2+} - doped biphasic hydroxyapatite/α-tricalcium phosphate obtained from hydrothermally synthesized Ag^{+} - and Cu^{2+} - doped hydroxyapatite. Appl Surf Sci 307:513–519
15. Remya NS, Syama S, Gayathri V, Varma HK, Mohanan PV (2014) An in vitro study on the interaction of hydroxyapatite nanoparticles and bone marrow mesenchymal stem cells for assessing the toxicological behaviour. Colloids Surf B 117:389–397
16. Byrne JD, Betancourt T, Brannon-Peppas L (2008) Active targeting schemes for nanoparticle system in cancer therapeutics. Adv Drug Deliv Rev 60:1615–1626
17. Wang SG, Li N, Pan W, Tang B (2012) Advances in functional fluorescent and luminescent probes for imaging intracellular small-molecular reactive species. Trends Anal Chem 39:3–37
18. Niu J, Wang X, Lv J, Li Y, Tang B (2014) Luminescent nanoprobes for in-vivo bioimaging. Trend Anal Chem 58:112–119
19. Kim J, Piao Y, Hyeon Y (2008) Multifunctional nanostructured materials for multimodel imaging, and simultaneous imaging and therapy. Chem Soc Rev 38:372–390
20. Peer D, Karp JM, Hong S, Farokhzad OC, Margalit R, Langer R (2007) Nanocarrers as an emerging platform for cancer therapy. Nat Nanotechnol 12:751–760
21. Lee SY, Jeon SI, Jung SH, Chung IJ, Ahn C-H (2014) Targeted multimodal imaging modalities. Adv Drug Deliv Rev 76:60–78
22. Norek M, Peters AJ (2011) MRI contrast agents on dysprosium or holmium. Prog Nucl Magn Reson Spectrosc 59:64–82
23. Xi D, Dong S, Meng X, Lu Q, Meng L, Ye J (2012) Gold nanoparticles as computerized tomography (CT) contrast agents. RSC Adv 2:12515–12524
24. Lusic H, Grinstaff MW (2013) X-ray-computed tomography contrast agents. Chem Rev 113:1641–1666
25. Ametamy SM, Honer M, Schubiger PA (2008) Molecular imaging with PET. Chem Rev 108:1501–1516
26. Li Z, Conti PS (2010) Radiopharmaceutical chemistry for positron emission tomography. Adv Drug Deliv Rev 62:1031–1051
27. Wades TJ, Wong EH, Weisman GR, Anderson CJ (2010) Coordinating radiometals of copper, gallium, indium, yttrium and zirconium for PET and SPECT imaging of disease. Chem Rev 110:2858–2902
28. Gobin AM, Lee MH, Halas NJ, James WD, Drezek RA, Weast JL (2007) Near-infrared resonant nanoshells for combined optical imaging and photothermal cancer therapy. Nano Lett 7:1929–1934
29. Fercher AF (2009) Optical coherence tomography-development, principles, applications. Z Med Phys 20:251–276
30. Pansare VJ, Hejazi S, Faenza W, Prudehomme RK (2012) Review of long-wavelength optical and NIR imaging materials: ontrast agents, fluorophores, and multifunctional nano carriers. Chem Mater 24:812–827
31. Harvey CJ, Blomley MJK, Eckersley RJE, Cosgrove DO (2001) Develpoements in ultrasound contrast media. Eur Radiol 11:675–689
32. Guo C, Jin Y, Dai Z (2014) Multifunctional ultrasound contrast agents for imaging guided photothermal therapy. Bioconjug Chem 25:840–854
33. Lu W, Huang Q, Ku G, Wen X, Zhou M, Guzatov D, Brecht P, Su R, Oraevsky A, Wang LV, Li C (2010) Photoacoustic imaging of living mouse brain vasculature using hollow gold nanospheres. Biomaterials 31:2617–2626
34. Savita N, Maitra S, Ravishankar U (2010) Multimodality molecular imaging – an overview with special focus on PET/CT. Apollo Med 7:190–199
35. Jennings L E, Long N J (2009) Two is better than one-probes for dual-modality molecular imaging. Chem Commun 3511–3524
36. Frullano L, Meade TJ (2007) Multimodal MRI contrast agents. J Biol Inorg Chem 12:939–949
37. Jadvar H, Colletti PM (2014) Competitive advantage of PET/MR. Eur J Radiol 83:84–94
38. Pichler B, Wehrl HF, Kolb A, Judenhofer MS (2008) Positron emission tomography/ magnetic resonance imaging: the next generation of multimodality imaging? Semin Nucl Med 38:199–208
39. Debasu ML, Ananias D, Pinho SLC, Geraldes CFGC, Carlos LD, Rocha J (2012) (Gd, Yb, Tb)PO_4 up -conversion nanocrystals for bimodal luminescence- MR imaging. Nanoscale 4:5154–5162
40. Qiao Z, Shi X (2014) Dendrimer-based molecular imaging contrast agents. Prog Polym Sci. doi:10.1016/j.progpolymsci.2014.08.002
41. Wolbeis O S (2015) An overview of nanoparticles commonly used in fluorescent bioimaging. doi:10.1039/c4cs00392f
42. Bae SW, Tan W, Hong J (2012) Fluorescent dye-doped silica nanoparticles: new tools for bioapplications. Chem Commun 48: 2270–2282
43. Wang X, Meier RJ, Wolfbis OS (2013) Fluorescent pH-sensitive nanoparticles in an agarose matrix for imaging of bacterial growth and metabolism. Angew Chem Int Ed 52:406–409
44. Tang R, Feng X (2014) Highly luminescent conjugated polymer nanoparticles for imaging and therapy. Can Chem Trans 1:78–84
45. Song Y, Zhu S, Yang B (2014) Bioimaging based on fluorescent carbon dots. RSC Adv 4:27184–27200
46. Yang Y (2014) Upconversion nanophosphores for use in bioimaging, therapy, drug delivery and bioassays. Microchim Acta 181:263–294
47. Cui M, Zhao Y, Song Q (2014) Synthesis, optical properties and applications of ultra-small luminescent gold nanoclusters. Trends Anal Chem 57:73–82
48. Caravan P, Ellison JJ, McMurry TJ, Lauffer RB (1999) Gadollinium(III) chelates as MRI contrast agents: structure, dynamics, and applications. Chem Rev 99:2293–2352
49. Nicolay K, Strijkers G, Grull H (2013) Gd- Containing nanoparticles as MRI contrast agents. In: Merbach A (ed) The chemistry of contrast agents in medical magnetic resonance imaging, 2nd edn. Wiley, UK, pp 449–483
50. Sharma P, Brown S, Walter G, Santra S, Moudgil B (2006) Nanoparticles for bioimaging. Adv Colloid Interf Sci 123:471–485

51. Lu X, Leng Y (2005) Theoretical analysis of calcium phosphate precipitation in simulated body fluid. Biomaterials 26:1097–1108
52. Sadat-Shojai M, Khorasani M, Dinpanah-Khoshdargi E, Jamshidi A (2013) Synthesis methods for nanosized hydroxyapatite with diverse structures. Acta Biomater 9:7591–7621
53. Liu D-M, Troczynski T, Tseng WJ (2001) Water-based sol–gel synthesis of hydroxyapatite:process development. Biomaterials 22:1721–1730
54. Salimi MN, Anuar A (2013) Charecterizations of biocompatible and bioactive hydroxyapatite particles. Procedia Eng 53:192–196
55. Wang J, Shaw L L (2009) Synthesis of high purity hydroxyapatite nanopowder via sol–gel combustion process. 20: 1223–1227
56. Han Y, Li S, Wang X, Chen X (2004) Synthesis and sintering of nanocrystalline hydroxyapatite powders by citric acid sol–gel combustion method. Mater Res Bull 39:25–32
57. Ruksudjarit A, Pengpat K, Rujijanagul G, Tunkasiri T (2008) Synthesis and characterization of nanocrystalline hydroxyapatite from natural bovine bone. Curr Appl Phys 8:270–272
58. Tabakovic A, Kester M, Adair JH (2012) Calcium phosphate-based composite nanoparticles in bioimaging and therapeutic delivery applications. WIREs Nanomed Nanobiotechnol 4:96–112
59. Talapin DV, Gaponik N, Borchert H, Rogach AL, Hasse M, Weller H (2002) Etching of colloidal InP nanocrystal with fluorides: photochemical nature of the process resulting in high photoluminescence efficiency. J Phys Chem B 106:12659–12663
60. Derfus AM, Chan WCW, Bhatia SN (2003) Probing the cytotoxicity of semiconductor quantum dots. Nano Lett 4:11–18
61. Zhang J, Fatouros PP, Shu C, Reid J, Qwens LS, Cai T, Gibson HW, Long GL, Corwin FD, Chen ZJ, Dorn HC (2010) High relaxivity trimetallic nitride (Gd_3N) metallofullerene MRI contrast agents with optimized functionality. Bioconjug Chem 21:610–615
62. Bunzil JG (2010) Lanthanide luminescence for biomedical analyse and imaging. Chem Rev 110:2729–2755
63. Bunzli J-CG, Eliseeva SV (2011) Basics of lanthanide photophysics. In: Haenninen P, Haerma H (eds) Lanthanide Luminescence: Photophysical, Analytical and Biological Aspects, Springer series on Fluorescence, vol 7. Springer, Heidelberg, pp 1–46
64. Eliseeva SV, Bunzil JG (2009) Lanthanide luminescence for functional materials and bio-sciences. Chem Soc Rev 39:189–227
65. Zhang Y, Wei W, Das GK, Tan TTY (2014) Engineering lanthanide-based materials for nanomedicine. J Photochem Photobiol C 20:71–96
66. Werts MHV (2005) Making sense of lanthanide luminescence. Sci Prog 88:101–131
67. Bunzil JC (2006) Benefiting from the unique properties of lanthanide ions. Acc Chem Res 39:53–61
68. Montogomery C P, Murray B S, New E J, Pal R, Parker D (2009) Cell-penetrating metal complex optical probes: targeted and responsive systems based on lanthanide luminescence. 42: 925–937
69. Wang S, Wang L Lanthanide-doped nanomaterials for luminescence detection and imaging. doi:10.1016/j.trac.2014.07.011
70. Fang Y, Xu A, Song R, Zhang H, You L, Yu J, Liu H (2003) Systematic synthesis and characterization of single-crystal lanthanide orthophosphate nanowires. J Am Chem Soc 125:16025–16034
71. Li C, Quan Z, Yang J, Lin J (2007) Highly uniform and monodisperse β-NaYF4:Ln3+(Ln=Eu, Tb, Yb/Er, and Yb/Tm) hexagonal microprism crystals: hydrothermal synthesis and luminescent properties. Inorg Chem 46:6329–6337
72. Wegh RT, Donker H, Oskam KD, Meijerink (1999) Visible quantum cutting in LiGdF4: Eu^{3+} through downconversion. Science 283:663–666
73. Mader HS, Kele P, Saleh SM, Wolfbeis OS (2010) Upconverting luminescent nanoparticles for use in biocojugation and bioimaging. Curr Opin Chem Biol 14:582–596
74. Chen G, Qiu H, Prasad PN, Chen X (2014) Upconversion nanoparticles: design, nanochemistry and applications in theranostics. Chem Rev 114:5161–5214
75. Weng M, Abbinei G, Clevenger A, Mao C, Xu S (2011) Upconversion nanoparticles: synthesis, surface modification and biological applications. Nanomed: Nanotechnol Biol Med 7:710–729
76. Auzel F (2004) Upconversion and anti-stokes processes with f and d ions in solids. Chem Rev 104:139–173
77. Heffern MC, Matosziuk LM, Meade TJ (2014) Lanthanide probes for bioresponsive imaging. Chem Rev 114:4496–4539
78. Doat A, Fanjul M, Pelle F, Hollande E, Lebugle A (2003) Europium-doped bioapatite: a new photostable biological probe, internalizable by human cells. Biomaterials 24:3365–3371
79. Ternane R, Ayedi MT, Ariguib NK, Piriou B (1999) Luminescent properties of Eu^{3+} in calcium hydroxyapatite. J Lumin 81:165–170
80. Cao XY, Wen F, Bian W, Cao Y, Pang C, Zhang W (2009) Preparation and comparison study of hydroxyl apatite and Eu-hydroxyapatite. Front Mater Sci 3:255–258
81. Kim EJ, Choi S, Hong S (2007) Synthesis and photoluminescence properties of Eu^{3+} -doped calcium phosphates. J Am Ceram Soc 9: 2795–2798
82. Huang S, Zhu J, Zhou K (2012) Effects of Eu^{3+} ions on the morphology and luminescence properties of hydroxyapatite nanoparticles synthesized by one-step hydrothermal method. Mater Res Bull 47:24–28. doi:10.1016/j.materresbull.2011.10.013
83. Long M, Hong F, Li W, Zhao H, Lv Y, Li H, Hu F, Sun L, Yan C, Wei Z (2008) Size-dependent microstructure and europium site preference influence fluorescent properties of Eu^{3+}-doped $Ca_{10}(PO_4)_6(OH)_2$ nanocrystal. J Lumin 128:428–436
84. Andre RS, Paris EC, Gurgel MFC, Rosa ILV, Paiva-Santos CO, Li MS, Varela JA, Longo E (2012) Structural evolution of Eu-doped hydroxyapatite nanorods monitored photoluminescence emission. J Alloys Comp 531:50–54
85. Liu Y, Tu D, Zhu H, Chen X (2013) Lanthanide-doped luminescent nanoprobes: controlled synthesis, optical spectroscopy, and bioapplications. Chem Soc Rev 42:6924–6959
86. Feng Z, Li Y, Huang Y, Seo HJ (2011) Luminescence properties of Eu^{2+} and Eu^{3+} doped calcium- deficient hydroxyapatite prepared in air. J Alloys Comp 509:7087–7092
87. Graeve OA, Kanakala R, Madadi A, Williams BC, Glass KC (2010) Luminescence variations in hydroxyapatites doped with Eu^{2+} and Eu^{3+} ions. Biomaterials 31:4259–4267
88. Sun Y, Yang H, Tao D (2012) Preparation and characterization of Eu3+ doped fluorapatite nanoparticles by a hydrothermal method. Ceram Int 38:6937–6941
89. Zhao Y, Zhu J, Zhu S, Huang Y, Li Z, Zhou K (2011) Synthesis and characterization of arginine modified europium-doped hydroxyapatite nanoparticle and its cell viability. Trans Nonferrous Metals Soc China 21:1773–1778
90. Wilusz RJ, Bednarkiewicz A, Strek W (2011) Synthesis and optical properties of Eu3+ ion doped nanocrystalline hydroxyapatite embedded in PMMA matrix. J Rare Earths 29:1111–1116
91. Popa CL, Ciobanu CS, Iconaru SL, Stan M, Dinischiotu A, Negrila CC, Heino MM, Guegan R, Predoi D (2014) Systematic investigation and in vitro biocompatibility studies on mesoporous europium doped hydroxyapatite. Cent Eur J Chem 12:1032–1046
92. Kattan AA, Dufour P, Ghys JD, Drouet C (2010) Preparation and physicochemical characteristics of luminescent apatite-based colloids. J Phys Chem C 114:2918–2924
93. Han Y, Wang X, Dai H, Li S (2013) Synthesis and luminescence of Eu^{3+} doped hydroxyapatite nanocrystallines: effects of calcinations and Eu^{3+} content. J Lumin 135:281–287
94. Hasna K, Kumar SS, Komath M, Varma MR, Jayaraj MK, Kumar KR (2013) Synthesis of chemically pure, luminescent Eu^{3+} doped

Hap nanoparticles: a promising fluorescent probe for in vivo imaging applications. Phys Chem Chem Phys 15:8106–8111
95. Wagner DE, Eisenmann KM, Nester-Kalinoski AL, Bhaduri SB (2013) A microwave-assisted solution combustion synthesis to produce europium-doped calcium phosphate nanowhiskers for bioimaging applications. Acta Biomater 9:8422–8432
96. Yang P, Quan Z, Li C, Kang X, Lian H, Lin J (2008) Bioactive, luminescent and mesoporous europium-doped hydroxyapatite as drug carrier. Biomaterials 29:4341–4347
97. Yan-zhong Z, Yan-yan H, Jun Z, Shai-hong Z, Zhi-you L, Ke-chao Z (2011) Characteristics of functionalized nano-hydroxyapatite and internalization by human epithelial cell. Nanoscale Res Lett 6:600–607
98. Sun R, Chen K, Wu X, Zhao D, Sun Z (2013) Controlled synthesis and enhanced luminescence of europium -doped fluorine-substituted hydroxyapatite nanoparticles. Cryst Eng Comm 15: 3442–3447
99. Escudero A, Calvo ME, Fernandez SR, de la Fuente JM, Ocana M (2013) Microwave-assisted synthesis of biocompatible europium-doped calcium hydroxyapatite and fluoroapatite luminescent nanospindles functionalized with poly(acrylic acid). Langmuir 29:1985–1994
100. Doat A, Pelle F, Gardant N, Lebugle A (2004) Synthesis of luminescent bioapatite nanoparticles for utilization as a biological probe. J Solid State Chem 177:1179–1187
101. Chen F, Zhu Y-J, Zhang K-H, Wu J, Wang K-W, Tang Q-L, Mo X-M (2011) Europium-doped amorphous calcium phosphate porous nanospheres: preparation and application as luminescent drug carriers. Nanoscale Res Lett 6:67–75
102. Dembski S, Milde M, Dyrba M, Schweizer S, Gellermann C, Klockenbring T (2011) Effect of pH on the synthesis and properties of luminescent SiO_2/calcium phosphate: Eu^{3+} core-shell nanoparticles. Langmuir 27:14025–14032
103. Li X, Zeng H, Teng L, Chen H (2014) Comparative investigation on the crystal structure and cell behavior of rare-earth doped fluorescent apatite nanocrystals. Mater Lett 125:78–81
104. Li L, Liu Y, Tao J, Zhang M, Pan H, Xu X, Tang R (2008) Surface modification of hydroxyapatite nanocrystallite by a small amount of terbium provides a biocompatible fluorescent probe. J Phys Chem C 112:12219–12224
105. Yang C, Yang P, Wang W, Wang J, Zhang M, Lin J (2008) Solvothermal synthesis and charecterization of Ln (Eu3+, Tb3+) doped hydroxyapatite. J Colloid Interface Sci 328:203–210
106. Hui J, Zhang X, Zhang Z, Wang S, Tao L, Wei Y, Wang X (2012) Fluoridated HAp : Ln^{3+} (Ln=Eu or Tb) nanoparticles for cell imaging. Nanoscale 4:6967–6970
107. Lebugle A, Pelle F, Charvillat C, Rousselot I, Chane-Ching J Y (2006) Colloidal and monocrystalline Ln^{3+} doped apatite calcium phosphate as biocompatible fluorescent probes. Chem Commun 606–608
108. Zhang X, Hui J, Yang B, Yang Y, Fan D, Liu M, Tao L, Wei Y (2013) PEGylation of fluorinated hydroxyapatite (FAp):Ln^{3+} nanorods for cell imaging. Polym Chem 4:4120–4125
109. Neumeier M, Halis LA, Davis SA, Mann S, Epple M (2011) Synthesis of fluorescent core-shell hydroxyapatite nanoparticle. J Mater Chem 21:1250–1254
110. Sun Y, Yang H, Tao D (2011) Microemulsion process synthesis of lanthanide-doped hydroxyapatite nanoparticles under hydrothermal treatment. Ceram Int 37:2917–2920
111. Liu H, Xi P, Xie G, Chen F, Li Z, Bai D, Zeng Z (2011) Biocompatible hydroxyapatite nanoparticles as a redox luminescence switch. J Biol Inorg Chem 16:1135–1140
112. de Araujo T S, Macedo Z S, de Oliveira P A S C, Valerio M E G (2007) Production and Characterization of pure and Cr^{3+}- doped hydroxyapatite for biomedical applications as fluorescent probes. 42: 2236–2243
113. Victor SP, Paul W, Jayabalan M, Sharma CP (2014) Supramolecular hydroxyapatite complexes as theranostic near-infrared luminescent drug carriers. Cryst Eng Comm 16:9033–9042
114. Liu H, Chen F, Xi P, Chen B, Huang L, Cheng J, Shao C, Wang J, Bai D, Zeng Z (2011) Biocompatible fluorescent hydroxyapatite: synthesis and live cell imaging applications. J Phys Chem C 115: 18538–18544
115. Ge X, Li C, Fan C, Feng X, Cao B (2013) Enhanced photoluminescence properties of methylene blue dye encapsulated in nanosized hyroyapatite/silica particles with core-shell structure. Appl Phys A 113:583–589
116. Morgan TT, Mudddana HS, Altinoglu EI, Rouse SM, Tabakovic A, Tabouillot T, Russin TJ, Shanmugavelandy SS, Butler PJ, Eklund PC, Yun JK, Kester M, Adair JH (2008) Encapsulation of organic molecules in calcium phosphate nanocomposite particles for intracellular imaging and drug delivery. Nano Lett 8: 4108–4115
117. Altinoglu EI, Russin TJ, Kaiser JM, Barth BM, Eklund PC, Kester M, Adair JH (2008) Near-infrared emitting fluorophore-doped calcium phosphate nanoparticles for in vivo imaging of human breast cancer. ACS Nano 2:2075–2084
118. Mokoena PP, Nagpure IM, Kumar V, Kroon RE, Olivier EJ, Neethling JH, Swart HC, Ntwaeaborwa OM (2014) Enhanced UVB emission and analysis of chemical states of $Ca_5(PO_4)_3OH$: Gd^{3+}, Pr^{3+} phosphor prepared by co-precipitation. J Phys Chem Solids 75:998–1003
119. Zhang C, Cheng Z, Yang P, Xu Z, Peng C, Li G, Lin J (2009) Architectures of strontium hydroxyapatite microspheres: solvothermal synthesis and luminescence properties. Langmuir 25:13591–13598
120. Zhang C, Li C, Huang S, Hou Z, Cheng Z, Yang P, Peng C, Lin J (2010) Self- activated luminescet and mesoporous strontium hydroxyapatite nanorods for drug delivery 31: 3374–3383
121. Naccache R, Rodriguez EM, Bogdan N, Sanz-Rodriguez F, Cruz MCI, Fuente AJ, Vetrone F, Jaque D, Sole JG, Capobianco JA (2012) High resolution fluorescence imaging of cancers using lanthanide ion-doped upconverting nanocrystals. Cancers 4:1067–1105
122. Cheng F, Sun K, ZhaoY LY, Xin Q, Sun X (2014) Synthesis and characterization of HA/YVO_4: Yb^{3+}, Er^{3+} up-conversion luminescent nano-rods. Ceram Int 40:1139–11334
123. Anuradha JJC, Gulati K, Ray A, Roy I (2014) Fluorophore-doped calcium phosphate nanoparticles for non-toxic biomedical applications. RSC Adv 4:40449–40455
124. Niemirowicz K, Markiewicz KH, Wilczewska AZ, Car H (2012) Magnetic nanoparticles as new diagnostic tools in medicine. Adv Med Sci 57:196–207
125. Yoo D, Lee J, Shin T, Cheon J (2011) Theranostic magnetic nanoparticles. Acc Chem Res 44:863–874
126. Laurent S, Forge D, Port M, Roch A, Robic C, Elst LV, Muller RN (2008) Magnetic iron oxide nanoparticles: synthesis, stabilization, vectorization, physicochemical characterization, and biological applications. Chem Rev 108:2064–2110
127. Reddy H, Arias JL, Nicolas J, Couvreur (2012) Magnetic nanoparticles: design and characterization, toxicity and biocompatibility, pharmaceutical and biomedical applications. Chem Rev 112: 5818–5878
128. Singamaneni S, Bliznyuk VN, Binek C, Tsymbal EY (2011) Magnetic nanoparticles: recent advances in synthesis, self-assembly and applications. J Mater Chem 21: 16819–16835
129. Gallo J, Long NJ, Aboagye EO (2013) Magnetic nanoparticles as contrast agents in the diagnosis and treatment of cancer. Chem Soc Rev 42:7816–7833

130. Gao J, Gu H, Xu B (2009) Multifunctional magnetic nanoparticles: design, synthesis, and biomedical applications. Acc Chem Res 42:1097–1107
131. Kaygili O, Dorozhkin SV, Ates T, Al-Ghamdi AA, Yakuphanoglu (2014) Dielectric properties of Fe doped hydroxyapatite prepare by sol–gel method. Ceram Int 40:9395–9402
132. Mercado DF, Magnacca G, Malandrino M, Rubert A, Montoneri E, Celi L, Prevot A, Gonzales MC (2014) Paramagnetic iron-doped hydroxyapatite nanoparticles with improved metal sorption properties. A bioorganic substrates-mediated synthesis. Appl Mater Interfaces 6:3937–3946
133. Liu X, Ma J, Yang J Visible-light-driven amorphous Fe(III)-substituted hydroxyapatite photocatalyst: Charecterization and photocatalytic activity. doi:10.1016/j.matlet.2014.09.018
134. Li Y, Ooi CP, Cheang PHN (2009) Synthesis and characterisation of neodymium (III) and gadolinium (III)- substituted hydroxyapatite as biomaterials. Int Appl Ceram Technol 4:501–512
135. Petchsang N, Pon-On W, Hodak JH, Tang IM (2009) Magnetic properties of Co-ferrite-doped hydroxyapatite nanoparticles having a core/shell structure. J Magn Magn Mater 321:1990–1995
136. Trandafir DL, Mirestean C, Turcu RVF, Frentiu B, Eniu D, Simon S (2014) Structural characterization of nanostructured hydroxyapatite-iron oxide composites. Ceram Int 40:11071–11078
137. Gopi D, Ansari MT, Shinyjoy E, Kavitha L (2012) Synthesis and spectroscopic charecterization of magnetic hydroxyapatite nanocomposite using ultrasonic irradiation. Spectrochim Acta A 87: 245–250
138. Low HR, Phonthammachai N, Stewart GA, Bastow TJ, Ma LL, White TJ (2008) The crystal chemistry of ferric oxyhydroxyapatite. Inorg Chem 47:11774–11782
139. Li Y, Widodo J, Lim S, Ooi CP (2012) Synthesis and cytocompatibility of manganese (II) and iron (III) substituted hydroxyapatite nanaoparticles. J Mater Sci 47:754–763
140. Liu Y, Sun Y, Cao C, Yang Y, Wu Y, Ju D, Li F (2014) Long-term biodistribution in vivo and toxicity of radioactive/ magnetic hydroxyapatite nanaorods. Biomaterials 35:3348–3355
141. Tampieri A, Iafisco M, Sandri M, Panseri S, Cunha C, Sprio S, Savini E, Uhlarz M, Herrmannsdorfer T (2014) Magnetic bioinspired hybrid nanostructured collagen- hydroxyapatite scaffolds supporting cell proliferation and tuning regenerative process. Appl Mater Interfaces. doi:10.1021/am5050967
142. Panseri S, Cunha C, Dalessandro T, Sandri M, Giavaresi G, Marcacci M, Hung CT, Tampieri A (2012) Intrinsically superparamagnetic Fe-hydroxyapatite nanoparticles positively influences osteoblast-like cell behaviour. J Nanobiotechnol 10:32–41
143. Ruixue S, Kezheng C, Lei X (2013) Preparation and Characterization of Hydroxyapatite/ -FE_2O_3 Hybrid Nanostructure. J Wuham Univ Technol Mater Sci Edu 215–219
144. Pon-On W, Meejoo S, Tang I (2008) Substitution of manganese and iron into hydroxyapatite: core/shell nanoparticle. Mater Res Bull 43:2137–2144
145. Iafisco M, Sandri M, Panseri S, Delgado-Lopez JM, Gomez-Morales J, Tampieri A (2013) Magnetic bioactive and biodegadable hollow Fe-doped hydroxyapatite coated poly(L-lactic) acid micro-nanospheres. Chem Mater 25:2610–2617
146. Tampieri A, DAlessandro T, Sandri M, Sprio S, Landi E, Bertinetti L, Panseri S, Pepponi G, Goettlicher J, Banobre-Lopez M, Rivas J (2012) Intrinsic magnetism and hyperthermia in bioactive Fe-doped hydroxyapatite. Acta Biomater 8:843–851
147. Kuda O, Pinchulk N, Iyanchenko L, Parkhomey O, Sych O, Leonowicz WR, Sowka E (2009) Effect of Fe_3O_4, Fe and Cu doping on magnetic properties and behaviour in physiological solution of biological hydroxyapatite/glass composite. J Mater Process Technol 209:1960–1964
148. Tseng C, Chang K, Yeh M, Yang K, Tang T, Lin F (2014) Development of a dual-functional Pt-Fe-HAP magnetic nanoparticles application for chemo-hyperthermia treatment of cancer. Ceram Int 40:5117–5127
149. Kanchana P, Lavanya N, Sekar C (2014) Development of amperometric L-tyrosine sensor based on Fe-doped hydroxyapatite nanoparticles. Mater Sci Eng C 35:85–91
150. Chandra VS, Baskar G, Suganthi RV, Elayaraja K, Joshy MIA, Beaula WS, Mythili R, Venkataraman G, Kalkura SN (2012) Blood compatibility of iron-doped nanosize hydroxyapatite and its drug release. Appl Mater Interfaces 4: 1200–1210
151. Ashokan A, Menon D, Nair S, Koyakkutty M (2010) A molecular receptor targeted, hydroxyapatite nanocrystals based multi-modal contrast agent. Biomaterials 31:2606–2616
152. Liu Z, Wang Q, Yao S, Yang L, Yu S, Feng X, Li F (2014) Synthesis and characterization of Tb^{3+}/Gd^{3+} dual-doped multifunctional hydroxyapatite nanaoparticle. Ceram Int 40:2613–2617
153. Li Z, Liu Z, Yin M, Yang X, Yuan Q, Ren JQX (2012) Aptamer-capped multifunctional mesoporous strontium hydroxyapatite nanovehicle for cancer-cell-responsive drug delivery and imaging. Biomacromolecules 13:4257–4263
154. Chen F, Huang P, Zhu Y, Wu J, Zhang C, Cui D (2011) The photoluminescence, drug delivery and imaging properties of multifunctional Eu^{3+}/Gd^{3+} dual-doped hydroxyapatite nanorods. Biomaterials 32:9031–9039
155. Ashokan A, Gowd GS, Somasundaram VH, Bhupathi A, Peethambaran R, Unni AKK, Palaniswami SP, Nair SV, Koyakkutty M (2013) Multifunctional calcium phosphate nanocontrast agent for combined nuclear, magnetic and near-infrared in vivo imaging. Biomaterials 34:7143–7157
156. Chen F, Huang P, Zhu Y, Wu J, Cui D (2012) Multifunctional Eu^{3+}/Gd^{3+} dual-doped calcium phosphate vesicle-like nanospheres for sustained drug release and imaging. Biomaterials 33: 6447–6455
157. Liu M, Liu H, Sun S, Li X, Zhou Y, Hou Z, Lin J (2014) Multifunctional hydroxyapatite/Na(Y/Gd)F_4:Yb^{3+}, Er^{3+} composite fibres for drug delivery and dual model imaging. Langmuir 30: 1176–1182
158. Syamchand SS, Priya S, Sony G (2015) Hydroxyapatite nanocrystals dually doped with fluorescent and paramagnetic labels for bimodal (luminomagnetic) cell imaging. Michrochim Acta 182:1213–1221
159. Yu MK, Park J, Jon S (2012) Targeting strategies for multifunctional nanoparticles in cancer imaging and therapy. Theranostics 2: 3–44
160. Veiseh O, Gunn JW, Zhang M (2010) Design and fabrication of magnetic nanoparticles for targeted drug delivery and imaging. Adv Drug Deliv Rev 62:284–304
161. Venkatasubbu GD, Ramasamy S, Avadhani GS, Ramakrishnan V, Kumar J (2013) Surface Modification and paclitaxel drug delivery of folic acid modified polyethylene glycol functionalized hydroxyapatite nanoparticles. Powder Technol 235:437–442
162. Yang Y, Liu C, Liang Y, Lin F, Wu K (2013) Hollow mesoporous hydroxyapatite nanoparticles (hmHANPs) with enhanced drug loading and pH-responsive release properties for intracellular drug delivery. J Mater Chem B 1:2447–2450
163. Wang S, Wang X, Xu H, Abe H, Tan Z, Zhao Y, Guo J, Naito M, Ichikawa H, Fukumori Y (2010) Towards sustained delivery of small molecular drugs using hydroxyapatite microspheres as the vehicles. Adv Powder Technol 21:268–272
164. Haifeng G, Zhiqiang Z, Feng Y, Guoping L, Zhiheng Z (2014) Preparation of magnetic, luminescent and mesoporous

hydroxyapatite nanospindles with high specific surface area. Rare Metal Mater Eng 43:2647–2651

165. Vuong QL, Doorslaer SV, Bridot JL, Argante C, Alejandro G, Hermann R, Disch S, Mattea C, Stapf S, Gossum Y (2012) Paramagnetic nanoparticles as potential MRI contrast agents: characterization, NMR relaxation, simulations and theory. Magn Reson Mater Phys 25:467–478

166. Guo D, Xu K, Zhao X, Han Y (2005) Development of a strontium - containing hydroxyapatite bone cement. Biomaterials 26:4073–4083